

1 Sedimentary insights into organic matter alteration in Arctic Alaska's 2 saline permafrost

3 Fabian Seemann^{1,2,3}, Michael Zech³, Maren Jenrich¹, Guido Grosse^{1,2}, Benjamin M. Jones⁴, Claire Treat⁵,
4 Lutz Schirmer¹, Susanne Liebner^{6,7} and Jens Strauss¹

5 ¹Permafrost Research Section, Alfred Wegener Institute Helmholtz Centre for Polar and Marine Research, 14473 Potsdam,
6 Germany

7 ²Institute of Geosciences, University of Potsdam, 14467 Potsdam, Germany

8 ³Institute of Geography, Technische Universität Dresden, 01069 Dresden, Germany

9 ⁴Institute of Northern Engineering, University of Alaska Fairbanks, Fairbanks, Alaska 99775, USA

10 ⁵Department of Agroecology, Aarhus University, 8000 Aarhus, Denmark

11 ⁶Institute of Biochemistry and Biology, University of Potsdam, 14467 Potsdam, Germany

12 ⁷GFZ Helmholtz Centre for Geosciences, Section Geomicrobiology, 14473 Potsdam, Germany

13 *Correspondence to:* Fabian Seemann (fabian.seemann@awi.de)

14 **Abstract.** In Arctic coastal lowland regions such as northernmost Alaska, thermokarst landscapes are often underlain by saline
15 ~~marine~~ deposits, a factor frequently overlooked when assessing permafrost thaw risks. To evaluate the influence of thaw and
16 salinity on organic matter degradation and landscape dynamics, we analyzed six sediment cores from representative landforms
17 near Utqiagvik (~~Barrow Peninsula~~, Alaska) using a multiproxy, carbon-focused approach, with emphasis on *n*-alkane
18 biomarkers. Undisturbed tundra uplands contained well-preserved, organic-rich Holocene sediments (~140 cm thick) overlying
19 brackish ~~late Pleistocene-Late Glacial~~ deposits, indicating the presence of saline permafrost. Thermokarst lake subsidence into
20 these substrates led to enhanced ~~organic matter carbon~~ degradation, as reflected by lower *n*-alkane carbon preference index
21 (CPI) values. While West Twin Lake talik sediments exhibited brackish porewater, East Twin Lake sediments were
22 characterized by predominantly saline porewater, indicating the presence of a cryopeg driven by salt-induced thaw-point
23 depression. Lagoonal environments, receiving both terrestrial and lacustrine inputs, accumulate sediments under unfrozen
24 hypersaline conditions, presenting a high potential for organic ~~matter decomposition carbon degradation~~. Carbon proxy
25 signatures statistically distinguish perennially frozen uplands, unfrozen lake ~~sediments~~, refrozen drained lake basins, and
26 lagoonal settings. Our results demonstrate that salt-bearing deposits, as found in all investigated sites, are vulnerable to active
27 layer deepening, talik and cryopeg formation, and ~~lake/coastal~~ shoreline erosion. These processes accelerate organic matter
28 degradation and alter landscape trajectories. Our study underscores the need to better understand the role of saline permafrost
29 in Arctic coastal lowlands and its broader implications under ongoing climate change.

30 **1 Introduction**

31 Arctic amplification is warming the polar north almost four times as fast as the global mean (Chylek et al., 2022; Rantanen et
32 al., 2022). This amplification contributes to permafrost warming, increasing active layer depths, and a shrinking permafrost
33 extent, which relates almost linearly to global warming (Biskaborn et al., 2019; Liu et al., 2024; McGuire et al., 2016; Nitzbon
34 et al., 2024; Smith et al., 2022). [With ~1460–1600 gigatons t](#) The terrestrial permafrost region stores about three times as much
35 organic carbon as global vegetation, which is vulnerable to [decomposition-mineralization](#) with warming temperatures and
36 permafrost thaw (Schuur et al., 2022; Strauss et al., 2025).

37 On vast Arctic coastal plains, like in northern Alaska, permafrost thaw manifests in several types of landforms, including
38 thermokarst lakes and lagoons. Thermokarst processes are accelerating in the Alaskan tundra (Chen et al., 2021), and Nitze
39 et al. (2017) describe a concurrent trend of thermokarst lake drainage. In drained lake basins (DLBs), permafrost starts to re-
40 aggrade, but as the climate continues to warm, taliks (unfrozen areas) may increasingly remain in the sediments (Farquharson
41 et al., 2022; Jones et al., 2022; [Lantz et al., 2022](#)).

42 Saline permafrost sediments are present under Holocene deposits on Arctic coastal plains, like in Alaska, Canada and Siberia
43 (Brigham-Grette and Hopkins, 1995; Brouchkov, 2002, 2003; Eisner et al., 2005; Osterkamp, 1989). In these sediments, which
44 were deposited [under-during](#) past [shallow-marine](#) [conditionstransgressions](#), the freezing point of pore ice is depressed due to
45 the high salt content, leading to a higher vulnerability to ground warming. When unfrozen cryotic deposits are present (i.e.,
46 unfrozen sediments at temperatures below the freezing point), these are referred to as cryopegs (van Everdingen, 2005). Jones
47 et al. (2023) for example observed intensified permafrost degradation as a thermokarst lake subsided into saline deposits. Such
48 trajectories are critical as the mobilization of previously freeze-locked organic matter occurs earlier than under non-saline
49 conditions, potentially enhancing carbon mineralization and greenhouse gas production in saline permafrost regions.

50 Along the coastlines, the combination of sea-level rise and erosion leads to significant land loss, altering the carbon cycle and
51 with that also greenhouse gas dynamics (Creel et al., 2024; Irrgang et al., 2022; Jenrich et al., 2024, 2025a; Nielsen et al.,
52 2022; Vonk et al., 2025). Coastal and gully erosion can lead to thermokarst lake drainage into the ocean but may also open up
53 lakes and turn them into new thermokarst lagoons (Arp et al., 2010; Jenrich et al., 2021; Jones et al., 2020). The importance
54 of such transitional environments is demonstrated by the abundance of lagoons along some coasts. For example, more than 70
55 % of the Alaskan Beaufort Sea coastline is characterized by both thermokarst and non-thermokarst lagoons (Harris et al., 2017;
56 Jenrich et al., 2025b).

57 To understand potential carbon losses due to permafrost degradation in such transitional landscapes, we need to understand
58 sediment properties from these complex and dynamic systems that are characterized by regular or saline permafrost and diverse
59 permafrost histories. On this issue, Giest et al. (2025) recently quantified a stronger [organic matter](#) degradation signal ([in the](#)
60 [context of microbial transformation toward a more mature state](#)) [in](#) of-saline deposits compared to non-salt-influenced sites by
61 [utilizing-using lipid biomarkersbiogeochemical-sediment-analyses](#). Since coastal permafrost regions can vary substantially in
62 their salinity - between fresh and hypersaline porewater conditions - (Jenrich et al., 2021), more differentiated investigations

63 across different salinity levels are needed. Organic carbon proxies such as organic carbon to nitrogen ratios (C:N), organic
64 carbon isotopes ($\delta^{13}\text{C}$, ^{14}C) and hydrocarbons (*n*-alkanes) are known to reflect organic matter origin and its degradation state,
65 making them useful tools in tracing paleoenvironmental change and present carbon dynamics in permafrost regions (e.g., Giest
66 et al., 2025; [Goñi et al., 2000](#); Strauss et al., 2015). Organic matter quality - in the sense of its future degradation potential -
67 can, for example, be assessed by the *n*-alkane carbon preference index (CPI), a proxy that is increasingly applied in permafrost
68 carbon studies (e.g., [Anderson et al., 2012](#); Haugk et al., 2022; [Martens et al., 2023](#); Yang et al., 2023).

69 In this study, we investigate the transformation of organic ~~matter carbon~~ during permafrost degradation by studying core
70 samples from a drilling transect along thaw and salinity gradients encompassing a diverse talik- and cryopeg-affected
71 thermokarst terrain in Arctic Alaska. Accordingly, we address the following research questions: (1) which paleoenvironmental
72 and modern processes and conditions shape today's sediment characteristics, (2) what is the organic matter quality in
73 thermokarst landforms on the [Utqiagvik Barrow](#) Peninsula, and (3) how do landscape dynamics affect organic matter
74 mobilization? To achieve this, we employ a sedimentary organic carbon-centered multiproxy approach, including the
75 aforementioned parameters.

76 2. Material and methods

77 2.1 Study area

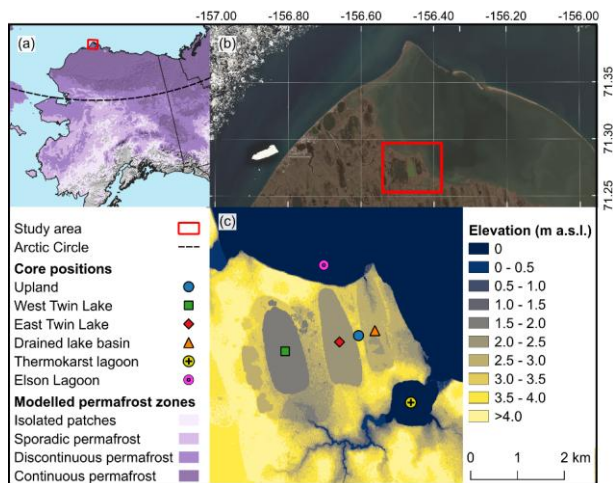
78 The study area lies ca. 10 km east of Utqiagvik (~~formerly Barrow~~: 71.276369-N, -156.452961-W; Fig. 1). The [Utqiagvik](#)
79 ~~Barrow~~ Peninsula covers an area of about 1800 km² (Lara et al., 2020). Geomorphologically, it is part of the Younger Outer
80 Coastal Plain, which belongs to the Arctic Coastal Plain (Hinkel et al., 2005).

81 In the period 2016-2020, the mean annual air temperature was -7.8 °C and the mean annual precipitation was 200 mm. Both
82 variables have been experiencing an ~~significant~~ increasing trend between 1981 and 2020 [by 1.1 °C decade⁻¹ and 23.1 mm](#)
83 [decade⁻¹, respectively](#) (Rawlins, 2021). The landscape is characterized by continuous permafrost with mean annual ground
84 temperatures of approx. -6 °C at the permafrost table (Obu et al., 2019). The permafrost thickness is about 400 m (Brown et
85 al., 2003) and the active layer (late season thaw) depth in Utqiagvik ranged between 29 cm and 47 cm in the monitoring period
86 1995-2019 (Nyland et al., 2021).

87 The ecoregion of the study area is Arctic Tundra (Lara et al., 2025). Tundra uplands (primary or remnant surfaces) are shaped
88 by high-centered polygons. High and flat centered polygons are dominated by graminoids, sedges and dwarf shrubs. Wet and
89 seasonally flooded positions such as DLBs and troughs are predominantly characterized by graminoid species, sedges and
90 *Sphagnum* mosses (Eisner et al., 2005; Lara et al., 2015; Wolter et al., 2024). The soil consists of ice- and organic-rich Holocene
91 deposits, which are underlain by late Pleistocene sandy and silty marine sediments (Eisner et al., 2005). These saline sediments
92 accumulated when sea levels were higher compared to today (Brigham-Grette and Hopkins, 1995; Brouchkov, 2003). The
93 Cretaceous bedrock consists of sedimentary rock (Black, 1964).

94 Thermokarst lakes cover about 22 % and DLBs 50 % of the landscape (Hinkel et al., 2003; Jones et al., 2022). Both lakes
 95 investigated in this study, Both in this study investigated lakes, West Twin Lake (1.3 km² surface area, 181 cm deep) and East
 96 Twin Lake (1.3 km² surface area, 175 cm deep) are characterized by floating ice regimes, yet West Twin Lake is a freshwater
 97 lake while East Twin Lake exhibits brackish water (Jones et al., 2023). In DLBs, permafrost reforms-aggradates after lake
 98 drainage, initializing polygonal patterns while remnant ponds may remain (Andresen and Lougheed, 2015; Eisner et al., 2005;
 99 Jones et al., 2022; Ling and Zhang, 2004). The former lake of the DLB, which is investigated in this study, was estimated to
 100 have drained about 100-150 years ago following coastal erosion (Brown et al., 2003). The erosion rate of Elson Lagoon north
 101 and east of the investigated terrestrial sites is 0.3-5.0 m yr⁻¹ per year (Gibbs and Richmond, 2017; Osterkamp and Harrison,
 102 1985). South of the DLB a semi-open thermokarst lagoon (0.8 km², 94 cm deep) is fed by multiple streams (Fig. 1). Elson
 103 Lagoon itself is a large (125 km²) but shallow (< 4 m) coastal lagoon with active deposition processes occurring (Zimmermann
 104 et al., 2022). Subsea permafrost exists beneath hypersaline lagoon sediments (Osterkamp and Harrison, 1982, 1985). The
 105 Barrow spit as well as barrier islands mark the transition to the Alaskan Beaufort Sea (Brown et al., 2003; Zimmermann et al.,
 106 2022).

hat formatiert: Hochgestellt



109 **Figure 1:** The study area located close to Utqiagvik at the North Slope of Alaska. (a) Alaskan permafrost extent map based on data
 110 from Obu et al. (2018), (b) Copernicus (2023) Sentinel-2 LA satellite image of the Utqiagvik Barrow Peninsula and Elson Lagoon,
 111 and (c) IFSAR digital terrain model (DGGs, 2018) with location of the coring sites. Map originally created by Lars Ebel.

hat formatiert: Schriftfarbe: Automatisch

112 2.2 Methods

113 2.2.1 Fieldwork

114 Sediment coring took place in April 2022. As the objective was to determine the transformation of organic ~~matter carbon~~
115 during permafrost thaw along a thaw and salt transect, coring positions were chosen ~~from form~~ the least thaw and salt affected
116 location, the upland, to the most thaw and salt affected sites, the lagoons. Fieldwork aimed at sampling near-surface and deep
117 (> 1 m) sediments, which was reached with the exception of coring at West Twin Lake (23 cm) and the semi-open ~~thermocarst~~
118 lagoon (46 cm). Detailed characteristics of core sites and metadata are provided in Table S1. Depending on the sediment
119 conditions, three different coring devices were used. Frozen material from the upland and the DLB sites were cored with a
120 “Snow, Ice and Permafrost Establishment” (SIPRE) corer. Since bedfast ice was present at Elson Lagoon and the semi-open
121 thermocarst lagoon, sediments were cored with a SIPRE corer, too. For transportation the cores were wrapped in plastic foil
122 and stored frozen in thermoboxes.

123 Unfrozen sediments of West Twin Lake were cored using a push corer (UWITEC gravity corer). Additionally, to get deeper,
124 East Twin Lake was sampled with a vibration coring system (Livingstone-type drive rod piston corer). These cores were kept
125 unfrozen in their PVC (push core) and aluminium (vibra core) tubes in thermoboxes for transportation to AWI (Potsdam,
126 Germany).

127 2.2.2 Multiproxy approach

128 In order to assess sediment characteristics along thaw and salinity gradients, a multiproxy approach was applied as individual
129 organic ~~matter carbon~~-proxies can be influenced by source heterogeneity, post-depositional alteration, and mixing of modern
130 and reworked deposits (Diefendorf et al., 2011; Jong et al., 2024; Wu et al., 2022). Combining complementary proxies therefore
131 allows robust interpretations of carbon sources, preservation states, and transformation processes.

133 Sample preparation

134
135 In preparation for the investigation of individual biogeochemical parameters, SIPRE cores were ~~processed treated~~ in a climate
136 chamber at -8°C. The lake cores were prepared at 4 °C. All cores were cut in halves, cleaned, photographed, and described
137 (sediment structures, color, cryostructures, Table S2-7). Subsequently, ~~sediment cores were subsampled~~ ~~subsamples were~~
138 ~~divided~~ in adjusted steps (approx. 5 cm intervals) following the sediment structure, and weighted. With the exception of East
139 Twin Lake, no artificial disturbances of the cores were observed.

141 Depth correction for vibra core compaction

142

143 During vibracoring of the East Twin Lake, especially sediments in the upper part of the lake deposits experienced compaction
144 due to high water content and extended vibration time, while the lower sediments were more consolidated and subjected to
145 less compaction. To correct the recovered core depths for compaction, a normalized exponential depth correction model was
146 applied, following Athy's law of exponential porosity–depth decay (Athy, 1930) and approaches used in ocean drilling studies
147 (Lisiecki and Herbert, 2007). The true sediment depth z_t was calculated from the measured depth z_m (in the core liner) using
148 the formula:

$$149 \quad z_t = D_p \times \frac{1 - e^{-z_m/\lambda}}{1 - e^{-L_c/\lambda}} \quad (1)$$

150 where D_p is the total penetration depth of the coring barrels (259 cm in this case), L_c is the total recovered core length (here
151 138 cm), and λ (lambda) is the exponential e-folding depth scale. The e-folding depth (λ) is defined as the characteristic depth
152 over which a quantity decreases to 1/e (approximately 37%) of its initial value, assuming an exponential compaction. In this
153 study, λ represents the depth scale at which sediment compaction effectively reduces porosity or thickness by a factor of e due
154 to vibration-induced consolidation. Based on previous studies of lakes, thermokarst properties were adapted (especially water
155 content, grain size, and porosity, e.g., Walter Anthony et al., 2014), and $\lambda = 50$ cm was assumed, reflecting the highly
156 compressible, water-rich upper layers. This correction ensures that the calculated true depth equals D_p at the base of the core
157 and follows an exponential compaction trend consistent with observed porosity–depth profiles in similar sediments.

158 **Porewater extraction and electrical conductivity measurements**

160
161 All samples were ~~kept~~continued to be treated at 4 °C. Porewater was extracted with Rhizon samplers (0.12-0.18 μm membrane
162 pore size). The extracted waters were measured with an Orion VERSASTAR PRO (Thermo Fisher) for electrical conductivity
163 (mS cm^{-1}). Salinity stages were adapted from Cahyadi et al. (2018) as follows: Freshwater < 1.5 mS cm^{-1} , brackish 1.5-15.0
164 mS cm^{-1} , saline 15.0-50.0 mS cm^{-1} , and hypersaline > 50 mS cm^{-1} . For subsequent sample treatment, the sediment remains
165 were freeze-dried, and the water/ice contents (in weight %, wt%) were calculated by taking into account the wet and dry sample
166 weights.

167 **Sedimentology and elemental analyses**

169
170 For the investigation of the grain size distribution, subsamples were treated with hydrogen peroxide for the removal of organic
171 matter for four weeks. The grain sizes were measured with a Malvern Mastersizer 3000 (0.01–1000 μm grain size range) and
172 evaluated with GRADISTAT 8.0 (Blott and Pye, 2001).

173 Using further subsamples, samples were milled and homogenized for the elemental analyses using a planetary mill (Fritsch
174 PULVERISETTE 5). Using a soliTOC and a rapid N exceed element analyzer (Elementar), total organic carbon (TOC) and
175 total nitrogen (TN) contents were quantified through the combustion and the analysis of the resulting gases. The detection

176 limits of TOC and TN are 0.001 wt% and 0.05 wt%, respectively, however, the detection limit was artificially set to 0.1 wt%
177 for both elements. TOC and TN contents below the detection limit (0.1 wt%) were replaced by half of the detection limit (0.05
178 wt%). This is to prevent a bias and is according to Strauss et al. (2022) to make the point that low measurements are not the
179 same as no measurements, avoiding zero inflation. For the TN samples below the detection limit, no C:N ratio calculation was
180 done to avoid artificial artifacts. The C:N ratio is a common [indirect](#) indicator of organic matter degradation [if assuming a](#)
181 [same source signal](#), with lower values reflecting higher decomposition (e.g., Fuchs et al., 2019; Mu et al., 2025). It also helps
182 to infer source material, distinguishing algal input (C:N < 10) from terrestrial plant matter (C:N > 20) (Meyers, 1994).

183 **Stable organic carbon isotope analysis**

184
185
186 Samples were decarbonized with hydrochloric acid before quantification of $\delta^{13}\text{C}$ at [the Alfred Wegener Institute's \(AWI\)'s](#)
187 ISOLAB facility. $\delta^{13}\text{C}$ ratios were measured using internationally certified reference materials obtained from the IAEA,
188 including USGS-24 (-15.99 ‰) and IAEA-CH-7 (-31.80 ‰). In addition, internal laboratory standards (peptone (-24.09 ‰)
189 and nicotinamide (-32.73 ‰)) were analyzed for quality control. Isotope values are reported in ‰ relative to Vienna Pee Dee
190 Belemnite (Coplen et al., 2006), and analytical precision was better than ± 0.15 ‰ based on repeated standard measurements
191 (Schwamborn et al., 2023). Measurements were run on a ThermoFisher Scientific Delta-V-Advantage gas mass spectrometer
192 equipped with a FLASH elemental analyser EA 2000 and a CONFLO IV gas mixing system. Stable carbon isotope ratios are
193 commonly applied as a proxy for organic matter origin and degradation in permafrost regions (e.g., Alewell et al., 2011; Strauss
194 et al., 2015).

195 **Radiocarbon dating**

196
197
198 Radiocarbon dating was conducted on 21 selected samples by accelerator mass spectrometry at the MICADAS radiocarbon
199 laboratory at AWI Bremerhaven (Mollenhauer et al., 2021). Preferably, plant remains were picked for dating, however, bulk
200 sediment was analyzed for four samples due to the lack of macrofossils (Table S8). Macrofossil material was subject to a
201 standard acid–base–acid pre-treatment ([Mollenhauer et al., 2021](#)). Subsequently, samples were rinsed to neutral pH, dried, and
202 combusted using an elemental analyzer. Owing to limited sample mass, all but two macrofossil samples (AWI MICADAS
203 sample ID 12532.1.1 and 12535.1.1, Table S8) were analyzed in gas mode rather than as graphite targets. Radiocarbon
204 measurements were normalized and blank-corrected using size-matched OxAlI and PhA standards. Data quality was monitored
205 using wood reference material (IAEA-C5) in parallel (Mollenhauer et al., 2021). The bulk solid phase samples were acidified
206 three times in silver boats with 6 M HCl to remove inorganic carbon. Radiocarbon dating was performed on 1 mgC graphite
207 targets. Sample treatment and blank determination was performed following existing protocols by Mollenhauer et al. (2021).
208 Raw radiocarbon ages were calibrated with Calib 8.20 using the IntCal 20 calibration curve (Reimer et al., 2020; Stuiver and
209 Reimer, 1993).

210

211 ***n*-Alkane biomarkers**

212

213 The total lipid extract from freeze-dried, milled and homogenized sediment was extracted with a Dionex ASE 350 Accelerated
 214 Solvent Extractor using dichloromethane/methanol (DCM/MeOH, 99:1 v/v, heating phase 5 min, static phase 20 min at 75°C
 215 and 10 MPa). Next, the internal standard 5 α -androstane was added to the extract. Asphaltenes were precipitated to avoid
 216 complications during the next step, where the *n*-alkane including aliphatic fraction was separated via medium pressure liquid
 217 chromatography using *n*-hexane over silica columns (Radke et al., 1980). This fraction was then measured using a Thermo
 218 Scientific ISQ 7000 Single Quadrupole Mass Spectrometer in combination with a Thermo Scientific Trace 1310 Gas
 219 Chromatograph (capillary column from BPX5, 2 mm \times 50 m, 0.25 mm). With a total run time of 118 min, the MS transfer line
 220 temperature was set to 250 °C and the ion source temperature to 230 °C (ionisation energy 70 eV at 50 μ A). Targeted screening
 221 of mid- and long chain *n*-alkanes (C₂₃-C₃₃) was realized with the software Xcalibur (Thermo Fisher). The mass spectra (*m/z*
 222 50-600 Da, 2.5 scans s⁻¹) and the internal standard were used for compound specific identification and quantification.

223

224 ***n*-Alkane proxies**

225

226 The total *n*-alkane content (TAC) is the first proxy that is indicative of (paleo) environmental conditions and degradation
 227 effects (e.g., Brittingham et al., 2017; Thomas et al., 2021). TAC is provided for the following chain lengths in $\mu\text{g } \mu\text{g}^{-1}$ Sediment
 228 (Sed) and $\mu\text{g } \mu\text{g}^{-1}$ TOC:

229
$$TAC = \sum C_{23} - C_{33} \tag{2}$$

230 The average chain length (ACL), developed by Poynter and Eglinton (1990), is a proxy that is indicative of the organic matter
 231 source. Algae and microorganisms are typically dominated by have short-chain *n*-alkanes (< C₂₂), aquatic (submerged/floating,
 232 e.g., *Sphagnum* moss) vegetation can be recognized by a dominance of mid-chain *n*-alkanes (C₂₃/C₂₅) while terrestrial
 233 vegetation is dominated by long-chain *n*-alkanes (> C₂₅) (Baas et al., 2000; Ficken et al., 2000; Killips and Killips, 2005; Otto
 234 and Simpson, 2005). Terrestrial vegetation can further be distinguished between shrubs and trees (C₂₇/C₂₉ predominance) and
 235 grasses and herbs (C₃₁/C₃₃ predominance) (Maffei, 1996; Schäfer et al., 2016). This chemotaxonomic “fingerprint”, as Eglinton
 236 et al. (1962) put it, can therefore be used as a tool for past environmental changes (e.g., Schwark et al., 2002; Zech et al., 2010).
 237 ACL limitations concern the blindness towards gymnosperms, overlapping chemotaxonomic patterns of different source
 238 material and potential post depositional alteration through degradation (Diefendorf et al., 2011; Jongejans et al., 2020; Struck
 239 et al., 2018; Zech et al., 2021). The ACL is calculated following Brittingham et al. (2017) and others:

240
$$ACL_{C_{23}-C_{33}} = \frac{\sum i \times C_i}{\sum C_i} \tag{3}$$

241 Odd chain alkanes predominate over even chain numbers (Eglinton et al., 1962). The ratio of odd against even chain lengths,
 242 called CPI, was first developed by Bray and Evans (1965) and further developed by Marzi et al. (1993). With advancing

hat formatiert: Hochgestellt

hat formatiert: Hochgestellt

hat formatiert: Tiefgestellt

hat formatiert: Tiefgestellt

243 organic matter decay this ratio decreases (e.g., Andersson and Meyers, 2012; Schäfer et al., 2016). The CPI values of algae,
244 bacteria, and highly degraded substances such as oil approach one while less degraded organic matter retains values > 5 (Haugk
245 et al., 2022; Killops and Killops, 2005; Tipple and Pagani, 2010). The CPI calculation is based on the formula introduced by
246 Marzi et al. (1993) for the chain length interval C₂₃₋₃₃-C₃₃.

$$247 \text{CPI}_{C_{23}-C_{33}} = \frac{\sum \text{odd } C_{23-31} + \sum \text{odd } C_{25-33}}{2 \times \sum \text{even } C_{24-32}} \quad (4)$$

249 To differentiate terrestrial vegetation between trees and shrubs (approaching 0), and grasses and herbs (approaching 1), the
250 endmember model of Schäfer et al. (2016) is applied:

$$251 n - \text{alkane ratio} = \frac{C_{31} + C_{33}}{C_{27} + C_{31} + C_{33}} \quad (5)$$

252 Ficken et al. (2000) developed a proxy (P_{aq}) which allows to more specifically quantify the share of aquatic macrophyte input
253 into the sedimentary record. Submerged/floating macrophytes reveal relatively high values (P_{aq} > 0.4) compared to emergent
254 and terrestrial plants (0.1 < P_{aq} < 0.4; P_{aq} < 0.1; respectively). To evaluate aquatic influences in the continuum from the
255 permafrost upland, over the thermokarst lakes and the drained basin, towards the lagoons, P_{aq} was applied accordingly:

$$256 P_{aq} = \frac{C_{23} + C_{25}}{C_{23} + C_{25} + C_{29} + C_{31}} \quad (6)$$

257 2.2.3 Statistical approaches

258 The combination of the biogeochemical and hydrochemical parameters was used to interpret units along the sediment cores
259 (described top-down, labelled in Roman numerals) to enhance clarity and facilitate understanding. Mean values are reported
260 alongside their standard deviations. Correlations between geochemical variables were assessed using Pearson correlation
261 analysis.

262 In order to statistically quantify the characteristics of organic matter parameters (TOC, C:N, δ¹³C) in different sediment
263 regimes, groups of thermal conditions (seasonally frozen, perennially frozen, unfrozen, refrozen, lagoon) and salinity stages
264 (freshwater, brackish, saline, hypersaline) were created. Due to violations of normality in multiple groups, as determined by
265 Shapiro-Wilk tests, the non-parametric Kruskal-Wallis test was used to assess differences in TOC, C:N, and δ¹³C among
266 groups. For subsequent pairwise comparisons of the categories with the parameters, Mann-Whitney U tests were applied,
267 coupled with the Benjamini-Hochberg (BH) p-value adjustment method. *n*-Alkane proxies were not included in the statistical
268 tests due to limited sample counts in individual groups.

269 To quantify if any group statistically differs from another based on the combination of TOC, C:N, and δ¹³C, a Permutational
270 Multivariate Analysis of Variance (PERMANOVA) was performed. Also, unique groups based on both their thermal and
271 salinity condition were created and tested with a PERMANOVA. Following a significant overall result, post-hoc pairwise
272 PERMANOVA tests were conducted with p-value adjustment (BH) to identify which specific groups differed. All statistical
273 analyses were carried out in RStudio and AI tools have been utilized for R coding.

hat formatiert: Tiefgestellt

hat formatiert: Tiefgestellt

hat formatiert: Tiefgestellt

hat formatiert: Schriftart: Kursiv

hat formatiert: Schriftart: Kursiv

hat formatiert: Schriftart: Kursiv

hat formatiert: Schriftart: Kursiv

hat formatiert: Schriftart: Kursiv

hat formatiert: Schriftart: Kursiv

hat formatiert: Schriftart: Kursiv

hat formatiert: Schriftart: Kursiv

hat formatiert: Schriftart: Kursiv

274 **3. Results**

275 **3.1 Biogeochemistry of the individual cores**

276 [The following subchapters are organized according to their geomorphological position. Chapter 3.2, by contrast, is structured](#)
277 [based on thermal and salinity differences.](#)

Formatiert: Standard

278 **3.1.1 Permafrost upland**

279 The upland core from the tundra site is characterized by silt-dominated ice-rich permafrost in the first two meters of the soil
280 column (on average 66.4±13.1 wt% ground ice; Fig. 2a). The electrical conductivity of the porewater indicates freshwater
281 conditions (< 1.5 mS cm⁻¹) and a trend towards saline conditions (max. 17.3 mS cm⁻¹) below 140 cm depth (Unit VI). At 75
282 and 102 cm depth, radiocarbon dating reveals similar ages with 6.98 and 6.97 cal ka BP, respectively, while a lower sample at
283 186 cm depth has an age of 13.263 cal ka BP. This suggests that Holocene deposits with a thickness of at least 126 cm (7.3 cal
284 ka BP) cover the underlying Late Pleistocene Glacial sediments. The TOC contents range between 35.3 wt% (Unit I) and 5.6
285 wt% (Unit VI). Between 70 and 100 cm depth, TOC contents are increased (Unit IV) compared to sediments above and below.
286 TN contents relate to TOC contents and range between 0.4 and 1.7 wt% (on average 0.7±0.3 wt%). Overall, the C:N ratio is
287 relatively homogenous along the core (on average 17.1±2.9). In the upper meter (Unit I-IV), the ratio is increased (19.7±1.5)
288 compared to the lower meter (14.4±0.5). Carbon isotopic values range from an average of -26.8±0.6 ‰ in the upper 48 cm
289 (Units I, II) to -27.7±0.4 ‰ between 53 and 198 cm depth. C:N and δ¹³C (r = 0.78, p < 0.001) correlate significantly (Fig. S1).
290 Total *n*-alkane contents FAC in the upland indicates a decreasing trend with depth (average 42.0±37.1 μg/g Sed; 268.7±160.7
291 μg/g TOC; Fig. 3a). The maximum content is found at 10 cm depth with 113.3 μg/g Sed (524.7 μg/g TOC) and the
292 minimum at 186 cm depth with 5.1 μg/g Sed (89.3 μg/g TOC). Long-chain *n*-alkanes dominate (average ACL 26.9±0.6)
293 and the degradation proxy CPI (average 15.1±4.4) reveals a distinct pattern. First, the CPI increases with depth from 10.6 to
294 21.5 (75 cm depth). Then, it drops to 10.0 (126 cm depth) and increases again to 15.6 (186 cm depth). The *n*-alkane ratio,
295 indicative for different terrestrial vegetation inputs, increases along the core from 0.1 (uppermost sample) to 0.4 (lowermost
296 sample). P_{aq} indicates aquatic influences with values between 0.4 and 0.7.

hat formatiert: Schriftart: Kursiv

hat formatiert: Hochgestellt

hat formatiert: Hochgestellt

hat formatiert: Hochgestellt

hat formatiert: Hochgestellt

hat formatiert: Hochgestellt

hat formatiert: Hochgestellt

297 **3.1.2 West Twin Lake**

298 The pushcore of the West Twin Lake talik is 23 cm long (4 subsamples) and therefore represents the surface sediments of the
299 thermokarst lake (Fig. 2b). The sediment consists of fine silt (mean grain size 5.04.8±0.2 μm) with porewater of slightly
300 brackish conditions (1.9 mS cm⁻¹). TOC contents are on average 16.1±0.4 wt%, and TN values range from below detection
301 limit to 0.9 wt%. This results in C:N ratios of 17.5 (8 cm depth), 17.4 (16 cm depth), and 18.9 (21 cm depth). The δ¹³C ratio
302 is on average -28.6±0.1 ‰.

303 One biomarker sample was analyzed at the West Twin Lake core at 8 cm depth (Fig. 3b). The total alkane content is 192.2 μg
304 g^{-1} Sed (1214.3 μg g^{-1} TOC) and is therefore higher than in the upland. On the other hand, the ACL (25.5) and CPI (6.9) are
305 lower compared to the upland. The *n*-alkane ratio, signaling terrestrial input into the lake, is 0.2, while the P_{aq} value is 0.8.

hat formatiert: Hochgestellt

hat formatiert: Hochgestellt

306 3.1.3 East Twin Lake

307 The sediments in the vibracore from the East Twin Lake are sandy to silty (Fig. 2c). Until 187 cm depth (Unit I, II) mean grain
308 sizes increase to 68.6 μm , and below that they average 16.4 \pm 6.1 μm . The electrical conductivity continuously increases from
309 brackish (14.1 mS cm^{-1} at 8 cm depth) to saline (43.3 mS cm^{-1} at 235 cm depth). Subsequently, the conductivity decreases but
310 remains in saline conditions. At 41 cm depth, radiocarbon dating revealed a Holocene age of 2,920 cal ka BP. At 215 and 252
311 cm depth, the sediment is of late Pleistocene age, 27,730 cal ka BP and 42,566 cal ka BP, respectively (Unit III). The surface
312 sediments have a TOC content of 16.0 wt% (Unit I). Subsequently, TOC decreases and remains < 3.0 wt% below 123 cm
313 depth (Unit II, III). Only six out of 26 samples showed TN values above the detection limit. The TN content in these samples
314 is 0.1-0.9 wt%. The resulting average C:N ratio is 9.9 \pm 6.1. Carbon isotopic values increase from a minimum of -28.9 ‰ at 41
315 cm depth to -25.7 ‰ at 197 cm depth. Below that, $\delta^{13}\text{C}$ values remain relatively homogenous until the core bottom at 258 cm
316 with an average of -25.8 \pm 0.1 ‰. C:N and $\delta^{13}\text{C}$ ($r = -0.91$, $p = 0.01$) reveal a very strong negative correlation (Fig. S1).

317 The surface sediment sample of East Twin Lake has a TAC of 305.4 μg g^{-1} Sed (2179.2 μg g^{-1} TOC), while at 75 and 121
318 cm depth, it decreased to 1.9 μg g^{-1} Sed (129.7 μg g^{-1} TOC) and 17.0 μg g^{-1} Sed (1020.0 μg g^{-1} TOC), respectively (Fig.
319 3e). Long-chain *n*-alkanes predominate (average ACL 26.0 \pm 0.5). CPI (average 6.2 \pm 0.8), *n*-alkane ratio (average 0.3 \pm 0.1), and
320 P_{aq} (0.7 \pm 0.1) are similar as in West Twin Lake.

hat formatiert: Hochgestellt

hat formatiert: Hochgestellt

hat formatiert: Hochgestellt

hat formatiert: Hochgestellt

hat formatiert: Hochgestellt

hat formatiert: Hochgestellt

321 3.1.4 Drained lake basin

322 The DLB core comprises frozen silty sand (Fig. 2d). The permafrost is less ice-rich compared to the upland (on average
323 48.8 \pm 20.6 wt% ground ice), and the electrical conductivity indicates predominantly brackish porewater conditions until 110
324 cm depth (on average 3.7 \pm 3.1 mS cm^{-1}). The basal surface peat (21 cm depth, Unit I), an indication of the drainage event date,
325 has an age of 0.7 cal ka BP. Between 74 and 108 cm depth, an age-depth inversion occurs with 10.5 and 9.9 cal ka BP,
326 respectively. The first late Pleistocene age is found at 140 cm depth with 34.1 cal ka BP. TOC values range between 1.5 (129
327 cm depth) and 42.4 wt% (undecomposed surface peat). Between 74 and 113 cm depth (Unit IV), a cryoturbated sediment
328 structure is found, which is characterized by organic-rich sediments (33.5 wt% TOC at 113 cm depth). The TN contents are in
329 the range of contents found in the upland, but are on average slightly lower (0.5 \pm 0.4 wt%). The C:N ratios (on average
330 18.6 \pm 5.1) reflect the TOC and TN patterns along the core; however, peak values (0-15 cm and 113 cm depth) are less dominant.
331 The $\delta^{13}\text{C}$ values increase with depth and range between -29.4 and -25.0 ‰ at 32.5 and 1376.5 cm depth, respectively. No
332 significant correlation is found between C:N and $\delta^{13}\text{C}$ ($r = -0.35$, $p = 0.08$; Fig. S1).

333 Compared to all investigated landforms, *n*-alkane specific parameters indicate the strongest heterogeneity in the DLB (Fig.
334 3e). TAC ranges between 0.9 μg g^{-1} Sed (38.6 μg g^{-1} TOC) and 519.8 μg g^{-1} Sed (3419.6 μg g^{-1} TOC), which is the lowest

hat formatiert: Hochgestellt

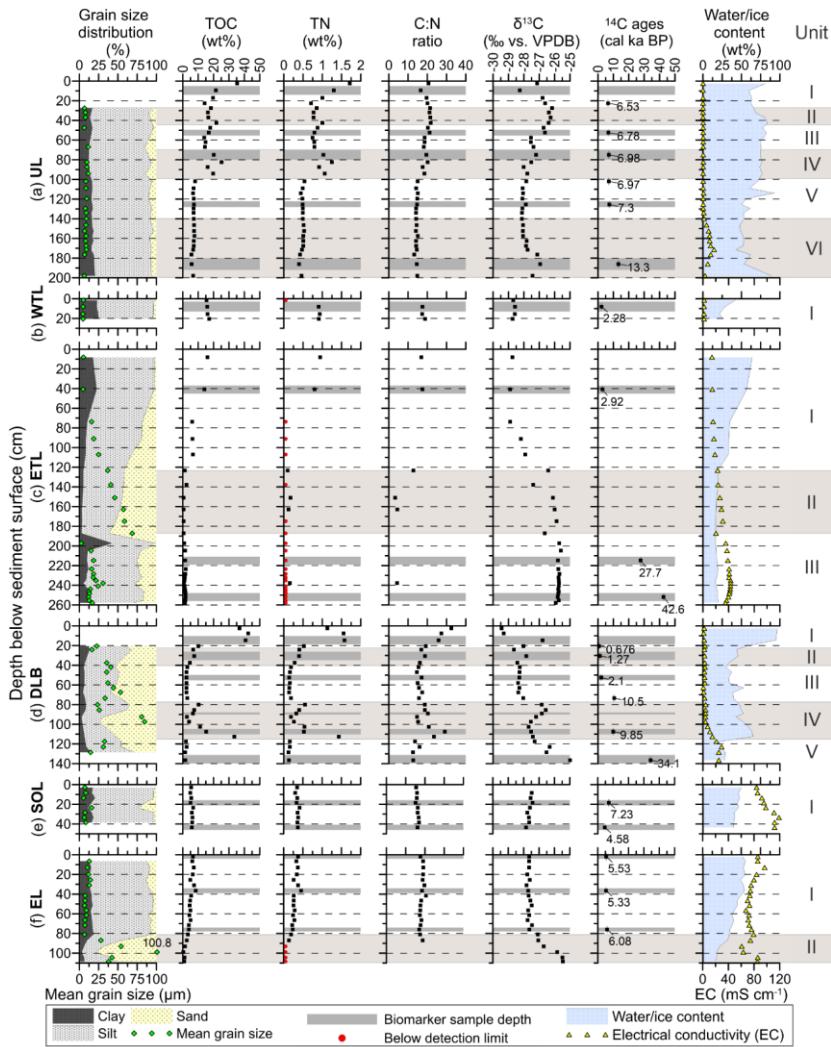
hat formatiert: Hochgestellt

hat formatiert: Hochgestellt

hat formatiert: Hochgestellt

335 and highest observed value in our study, respectively. The minimum ACL (25.6 at 31 cm depth) is similar to the surface
336 samples of the ~~twin~~-lakes. At 108 cm depth, extreme values are reached for ACL (30.2), CPI (51.3), the terrestrial *n*-alkane
337 ratio (0.9), and P_{aq} (0.02).

338



339
 340 **Figure 2: Sedimentological, elemental, isotopic and hydrochemical data from the investigated sediment cores: (a) UL (upland, 204**
 341 **cm core length), (b) WTL (West Twin Lake, 23 cm core length), (c) ETL (East Twin Lake, 259 cm core length), (d) DLB (drained**
 342 **lake basin, 142 cm core length), (e) SOL (semi-open, thermokarst lagoon, 46 cm core length), (f) EL (Elson Lagoon, 110 cm core**
 343 **length). Core units are based on parameter interpretation.**

hat formatiert: Schriftfarbe: Automatisch

hat formatiert: Schriftfarbe: Automatisch

hat formatiert: Schriftfarbe: Automatisch

hat formatiert: Schriftfarbe: Automatisch

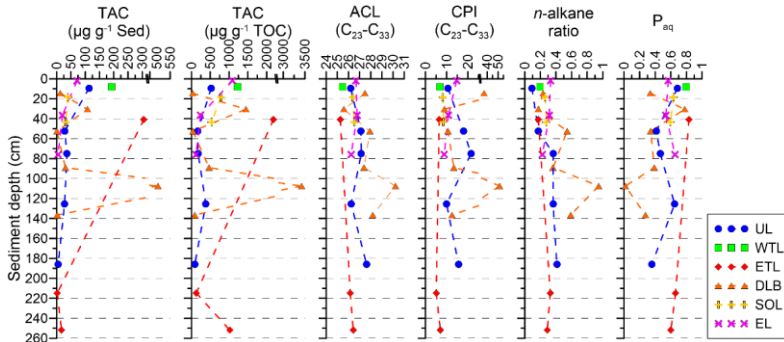


Figure 3: *n*-Alkane proxies along sediment cores: total *n*-alkane content (TAC) in $\mu\text{g g}^{-1}$ sediment (Sed) and $\mu\text{g g}^{-1}$ total organic carbon (TOC), average chain length (ACL), carbon preference index (CPI), *n*-alkane ratio and P_{aq} . The sediment cores comprise UL (upland, blue circle), WTL (West Twin Lake, green square), ETL (East Twin Lake, red diamond), DLB (drained lake basin, orange triangle), SOL (semi-open thermokarst lagoon, yellow plus), and EL (Elson Lagoon, magenta cross).

3.1.5 Semi-open thermokarst lagoon

The thermokarst lagoon core contains silty sediments (Fig. 2e). The average water content is of 44.4 ± 3.6 wt% and the porewater is characterized by hypersaline conditions with a peak value of 119.0 mS cm^{-1} at 34 cm depth. Radiocarbon dating of plant macrofossils shows an age-depth inversion with 7.2 cal ka BP at 19 cm depth and 4.6 cal ka BP at 44 cm depth. The TOC and TN contents average 5.8 ± 0.6 wt% and 0.4 ± 0.0 wt%, respectively. This results in an average C:N ratio of 16.1 ± 0.6 . Relatively homogenous values are also found for $\delta^{13}\text{C}$ with an average of -27.6 ± 0.1 ‰. C:N and $\delta^{13}\text{C}$ ($r = -0.50$, $p = 0.17$) are not correlating significantly (Fig. S1).

The two analyzed biomarker samples in the semi-open thermokarst lagoon are similar (Fig. 3e). A TAC of 40.0 $\mu\text{g g}^{-1}$ Sed (784.8 $\mu\text{g g}^{-1}$ TOC) and 31.5 $\mu\text{g g}^{-1}$ Sed (534.7 $\mu\text{g g}^{-1}$ TOC) is present at 19 and 44 cm depth, respectively. The average ACL (26.4 ± 0.1) and CPI (8.3 ± 0.1) lie between the observed values of the thermokarst lakes and the terrestrial sites. Also, the terrestrial *n*-alkane ratio (average 0.3 ± 0.0), and P_{aq} (average 0.6 ± 0.0) are within the range of values observed in the other cores.

3.1.6 Elson Lagoon

The Elson Lagoon core comprises silty sediments underlain by sand (Fig. 2f). The maximum and minimum porewater contents are 55.8 and 16.6 wt% at 7 and 109 cm depth, respectively. Compared to the thermokarst lagoon, Elson Lagoon is less saline, yet hypersaline conditions prevail (on average 76.2 ± 8.7 mS cm^{-1}). Radiocarbon ages signalize sediment mixing as plant macrofossils have an age of 5.5 cal ka BP at 2 cm depth and 5.3 cal ka BP at 37 cm depth. Along the core, TOC contents are

hat formatiert: Englisch (Vereinigte Staaten)

hat formatiert: Englisch (Vereinigte Staaten)

Formatiert: Standard (Web), Block, Rahmen: Oben: (Kein Rahmen), Unten: (Kein Rahmen), Links: (Kein Rahmen), Rechts: (Kein Rahmen), Zwischen: (Kein Rahmen)

hat formatiert: Schriftart: Kursiv

hat formatiert: Schriftart: 9 Pt., Englisch (Vereinigte Staaten)

hat formatiert: Englisch (Vereinigte Staaten)

hat formatiert: Schriftart: 9 Pt., Englisch (Vereinigte Staaten)

hat formatiert: Englisch (Vereinigte Staaten)

hat formatiert: Schriftart: 9 Pt., Englisch (Vereinigte Staaten)

hat formatiert: Englisch (Vereinigte Staaten)

hat formatiert: Englisch (Vereinigte Staaten)

hat formatiert: Englisch (Vereinigte Staaten)

hat formatiert: Englisch (Vereinigte Staaten)

hat formatiert: Englisch (Vereinigte Staaten)

hat formatiert: Englisch (Vereinigte Staaten)

hat formatiert: Englisch (Vereinigte Staaten)

hat formatiert: Englisch (Vereinigte Staaten)

hat formatiert: Englisch (Vereinigte Staaten)

hat formatiert: Englisch (Vereinigte Staaten)

hat formatiert: Englisch (Vereinigte Staaten)

hat formatiert: Englisch (Vereinigte Staaten)

hat formatiert: Englisch (Vereinigte Staaten)

hat formatiert: Hochgestellt

hat formatiert: Hochgestellt

hat formatiert: Hochgestellt

hat formatiert: Hochgestellt

367 on average 4.5 ± 2.2 wt% and show a decreasing trend. Until 87 cm depth, TN averages 0.3 ± 0.1 wt%, and contents are < 0.1
 368 wt% below this depth. The C:N ratio is relatively homogenous with an average of 18.4 ± 0.9 . $\delta^{13}\text{C}$ lies on average at -27.7 ± 0.1
 369 ‰ until 76 cm depth (Unit I). From 81 to 109 cm depth (Unit II) $\delta^{13}\text{C}$ precipitously increases to -25.4 ‰, which is the maximum
 370 value compared to all cores. No **significant** correlation is found between C:N and $\delta^{13}\text{C}$ ($r = -0.26$, $p = 0.32$; Fig. S1).
 371 The sediments of Elson Lagoon reveal a decreasing trend of TAC with depth (average $32.1 \pm 28.5 \mu\text{g/g}^{-1}$ Sed; $483.9 \pm 432.2 \mu\text{g}$
 372 g^{-1} TOC; Fig. 3f). *n*-Alkane proxies compare generally well to the thermokarst lagoon with the exception of the CPI. The
 373 degradation proxy indicates less degraded material (average 11.4 ± 2.4) in the non-thermokarst lagoon compared to the
 374 thermokarst lagoon. Otherwise, the average ACL (26.6 ± 0.2), terrestrial *n*-alkane ratio (0.3 ± 0.0), and P_{aq} (0.6 ± 0.0) are similar
 375 as in the **semi-open-thermokarst** lagoon.

hat formatiert: Hochgestellt

hat formatiert: Hochgestellt

376 3.2 Influence of temperature and salinity

377 3.2.1 Thermal sediment stages

378 Our five thermal sediment stages comprise *seasonally frozen* (including the max. active layer depths of **the upland** (UL) and
 379 **the DLB** after Nyland et al. (2021)), *perennially frozen* (referring to the permafrost domain of **the upland** (UL), *unfrozen*
 380 (talik/cryopeg of West and East Twin Lake), *refrozen* (corresponding to DLB permafrost sediments), *unfrozen* (talik/cryopeg
 381 of West and East Twin Lake), and *lagoon* (thermokarst lagoon and Elson Lagoon sediments) (for details see Table S9).

382 Kruskal-Wallis tests show that significant differences exist among the thermal regimes for TOC ($p < 0.001$), C:N ($p < 0.001$),
 383 and $\delta^{13}\text{C}$ ($p = 0.02$) (Table S9). Significance levels of pairwise Mann-Whitney test results are visualized in Fig. 4. The
 384 PERMANOVA test considering the combination of TOC, C:N and $\delta^{13}\text{C}$ indicated significant differences between thermal
 385 regimes ($r = 0.40$, $p = 0.001$). Post-hoc testing revealed that *unfrozen* sediments are significantly different from *frozen* ($r =$
 386 0.40 , $p = 0.05$), *refrozen* ($r = 0.55$, $p = 0.02$), and *lagoon* sediments ($r = 0.40$, $p = 0.04$). *Frozen* sediments further differ from
 387 *refrozen* ($r = 0.40$, $p = 0.03$) and *lagoon* ($r = 0.55$, $p = 0.01$) sediments. Also, significant differences exist between *refrozen*
 388 and *lagoon* sediments ($r = 0.40$, $p = 0.03$).

389 **Table 1: Grouping of sediment samples into thermal stages. Sample count (*n*) in individual groups with reduced number after *n/a***
 390 **removal in brackets (only samples with complete TOC, C:N, and $\delta^{13}\text{C}$ data were included in the statistical analyses). UL – Upland,**
 391 **WTL – West Twin Lake, ETL – East Twin Lake, DLB – Drained lake basin, SOL – Semi-open thermokarst lagoon, EL – Elson**
 392 **Lagoon.**

Thermal stage	UL		WTL		ETL		DLB		SOL		EL		total	
	#	depth (cm)	#	depth (cm)	#	depth (cm)	#	depth (cm)	#	depth (cm)	#	depth (cm)	#	depth (cm)
seasonally frozen	8	3-43					9	3-47						17
perennially	26	48-198												26

frozen							
unfrozen	4 (3)	2-21	26 (6)	8-258	30 (9)		
refrozen			17	53-137	17		
lagoon			10 (9)	3-131	21 (17)	2-109	31 (26)

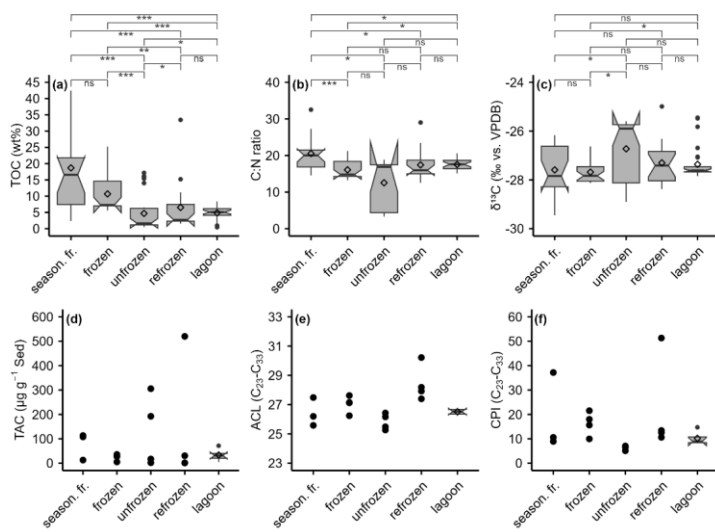


Figure 4: Notched boxplots of organic geochemical carbon-parameters across based on thermal regimes. Boxplots are shown for sample counts >4 and include n medians (center lines), interquartile ranges (IQR, 25th-75th percentile), whiskers ($1.5 \times$ IQR), outliers (points), and means (diamonds). Notches display the 95 % confidence interval. Significance brackets in panel a-c comprise the significance levels $p < 0.001$ (***), $p < 0.01$ (**), $p < 0.05$ (*) and $p > 0.05$ (ns), for sample counts >4. Sediment classes comprise seasonally frozen (season. fr.), frozen (fr.), unfrozen (unfr.), refrozen (refr.) and lagoon (lag.). Significance brackets are plotted for (a) TOC, (b) C:N (c) $\delta^{13}\text{C}$, and comprise the significance levels $p < 0.001$ (***), $p < 0.01$ (**), $p < 0.05$ (*) and $p > 0.05$ (ns).

3.2.2 Salinity stages

Grouping of sediment samples was conducted after previously defined salinity stages (section 2.2.2, for details see Table S102).

Significant differences in TOC ($p < 0.001$), C:N ($p < 0.001$), and $\delta^{13}\text{C}$ ($p < 0.001$) exist across at least some of the defined salinity stages according to Kruskal-Wallis (Table S10). Pairwise Mann-Whitney test significant levels are plotted in Fig. 5.

PERMANOVA testing indicated that significant differences in salinity categories exist ($r = 0.55$, $p = 0.001$). Post-hoc testing revealed weak but significant differences between brackish and hypersaline samples ($r = 0.07$, $p = 0.05$).

- hat formatiert: Schriftfarbe: Automatisch
- hat formatiert: Schriftfarbe: Automatisch
- hat formatiert: Schriftfarbe: Automatisch
- hat formatiert: Schriftfarbe: Automatisch
- hat formatiert: Schriftfarbe: Automatisch
- hat formatiert: Schriftfarbe: Automatisch
- hat formatiert: Schriftfarbe: Automatisch
- hat formatiert: Schriftfarbe: Automatisch
- hat formatiert: Schriftfarbe: Automatisch
- hat formatiert: Schriftfarbe: Automatisch

424 other concerning TOC, C:N and $\delta^{13}\text{C}$ ($r = 0.58$, $p = 0.001$). Post-hoc pairwise PERMANOVA tests revealed that Group 2 and
425 Group 6 were significantly different ($r = 0.87$, $p = 0.03$). Also, Group 3 differed significantly from Group 9 ($r = 0.87$, $p < 0.01$).

426 **Table 1.3: Grouped thermal and salinity regimes and contributing cores. Sample count (n) in individual groups with reduced number**
427 **after n/a removal in brackets (only samples with complete TOC, C:N, and $\delta^{13}\text{C}$ data were included in the statistical analyses).**
428 **Asterisks mark small group sizes (< 5). These groups were not considered in the PERMANOVA analyses. UL - Upland, WTL - West**
429 **Twin Lake, ETL - East Twin Lake, DLB - Drained lake basin, SOL - Semi-open thermokarst lagoon, EL - Elson Lagoon.**

hat formatiert: Schriftfarbe: Automatisch

hat formatiert: Schriftfarbe: Automatisch

Group	Thermal regime	Salinity stage	Contributing core	n
G1	seasonally frozen	freshwater	UL, DLB	9
G2	seasonally frozen	brackish	DLB	8
G3	frozen	freshwater	UL	16
G4	frozen	brackish	UL	9
G5	frozen	saline	UL	1*
G6	unfrozen	brackish	WTL, ETL	6 (5)
G7	unfrozen	saline	ETL	24 (4)*
G8	refrozen	freshwater	DLB	2*
G9	refrozen	brackish	DLB	11
G10	refrozen	saline	DLB	4*
G11	lagoon	hypersaline	SOL, EL	31 (26)

430

431 4. Discussion

432 4.1 Modern and paleoenvironmental processes and conditions

433 The biogeochemistry of the investigated landforms provides insights into the landscape history and current environmental
434 conditions.

435 4.1.1 Permafrost upland

436 The recent active layer depth in the tundra ranges between 29 cm and 47 cm (Nyland et al., 2021). This aligns well with the
437 increased TOC and TN contents of Unit I (Fig. 2a). Measured electrical conductivity in the sediments reflects freshwater
438 conditions, consistent with observations from the same upland (Jones et al., 2023) and in nearby streams (Lougheed et al.,
439 2020). Unit II represents the range of the late-season thaw depth and the transient layer, which can be recognized by increased
440 water/ice contents (Shur et al., 2005). The permafrost begins below 47 cm (Unit III). Bockheim et al., (1999) found that > 75
441 % of soils in the region are affected by cryoturbation; signs for this are found between 70 and 100 cm depths (Unit IV, Table

442 S2). TOC and TN contents are increased compared to the units above and below, and the radiocarbon dates reveal an age-
443 depth inversion. Cryoturbation at this depth could point towards a paleo active layer from the mid Holocene. Relatively
444 homogenous conditions in the second meter (Unit V, VI) indicate fairly stable conditions from the Late Glacial into the early
445 Holocene period.

446 Through the investigation of pollen records, Meyer et al. (2010) describe a shift from a purely grass dominated tundra in the
447 Late Glacial towards a grass, sedge, and dwarf shrub mix in the early Holocene. Considering the terrestrial *n*-alkane proxies
448 ACL and the *n*-alkane ratio, it could be inferred that this slowly occurring shrubification throughout the Holocene can be
449 confirmed by our *n*-alkane analysis due to the tendency towards lower ACL and *n*-alkane ratio values in Holocene samples
450 compared to the deepest (Late Glacial) biomarker sample (Fig. 3a). Furthermore, an aquatic influence indicated by the P_{aq}
451 (section 3.3.1) may be explained by the presence of *Sphagnum* moss in ice-wedge troughs (Lara et al., 2015). However, P_{aq}
452 could also be affected by mid-chain-length dominated *Betula* shrubs, whose *n*-alkane distributions can overlap with those of
453 aquatic vegetation, limiting its source specificity (Ficken et al., 2000; Weber and Schwark, 2020).

454 4.1.2 Thermokarst lakes

455 Different from the gradual top-down thaw processes in the upland, thermokarst lakes are affected by abrupt thaw processes
456 which can reach ~~much~~ deeper deposits over short time scales (Grosse et al., 2011; Webb et al., 2025). While uplands and
457 thermokarst lakes are sedimentologically connected due to the same parent material, the biogeochemical fingerprints of lakes
458 may have changed due to recent thaw processes and lacustrine deposition. Comparing our two lake sites is challenging, as the
459 West Twin Lake core is short, thus, a full comparison to the longer East Twin Lake core is somewhat limited. The main
460 difference lies in the salinity between the lake sediments. While brackish conditions occur beneath West Twin Lake, the
461 sediments of East Twin Lake have predominantly saline porewater (Fig. 2b, c; ~~Table 2~~). In East Twin Lake, electrical
462 conductivity was observed to have almost tripled between 2016 and 2022 (Jones et al., 2023). As negative temperatures were
463 measured in these sediments (Jones et al., 2023), we defined the unfrozen sediments as a cryopeg. Since brackish talik
464 sediments were determined in the freshwater West Twin Lake, a near-future shift towards brackish lake water is likely. East
465 Twin Lake's sediments (ca. 123 cm, Unit I) can be distinguished from the underlying late Pleistocene marine ~~influenced~~
466 sediments (Unit III) by considering the TOC contents (Eisner et al., 2005). These are in the range of values observed in the
467 Teshepuk Lake area, ca. 120 km east of the [Utqiagvik Barrow](#)-Peninsula (Lenz et al., 2016). P_{aq} indicates an increased aquatic
468 influence in the upper sediments. Yet ACL and the *n*-alkane ratio also indicate terrestrial plant input into the lake which can
469 be explained by enhanced lateral expansion (shoreline erosion) in recent years (Jones et al., 2023). It needs to be stressed that
470 in our study the ACL decreases with decreasing CPI values ($r = 0.79$, $p < 0.001$), meaning that the vegetation signal is
471 influenced by organic matter degradation (strongest in ~~East Twin Lake TL~~).

472 The transition from Unit II to III ~~in the East Twin Lake core~~ is characterized by a sharp decrease of the mean grain size from
473 fine sand to silt. The sand might be aeolian which deposited in the surface depression (Carter, 1981; Eisner et al., 2005). In
474 both units, the C:N and $\delta^{13}C$ ratios point towards a marine/lacustrine algae production (Fig. 4b, c; Meyers, 1994), which aligns

475 with the high salinity ~~and the radiocarbon dates~~ (Figure 2c, ~~Table S8~~). This pattern matches with the investigation of Meyer et
476 al. (2010), who observed more enriched $\delta^{13}\text{C}$ values in the salty late Pleistocene sediments at a permafrost tunnel on the
477 [Utqiagvik Barrow](#) Peninsula.

478 4.1.3 Drained lake basin

479 In view of the landscape alteration, the next step is the drainage of thermokarst lakes ~~with where~~ permafrost ~~aggregation is re-~~
480 ~~forming at subaerial conditions~~. The DLB core revealed mixed signals. Electrical conductivity is similar to the upland, which
481 is linked to Holocene ages, whereas the sediments are sandier, comparable to the East Twin Lake sediments. Brown et al.
482 (2003) estimated that the lake drained about 100-150 years ago; however, our radiocarbon dating revealed that post-drainage
483 peat formation was initiated ca. 700 cal BP (Fig. 2d). DLBs sequester organic carbon in the form of peat (Bockheim et al.,
484 2004; Hinkel et al., 2003; Jones et al., 2012), which can be recognized by the highest TOC contents and C:N ratios in the upper
485 15 cm (Unit I). We argue that the most recent lake phase in the DLB started 1.3 cal ka BP and therefore lasted only
486 approximately 600 years when considering the TOC contents (Unit II). Between 21 and 31 cm depth, TOC contents are in the
487 range of contents found in the East Twin Lake sediments, and P_{aq} signalizes aquatic conditions. Our observation of the former
488 lake phase shows that these periods are in this case shorter than previously estimated by Fuchs et al. (2019), who found that
489 lakes persist a minimum of 1000 years in northern Alaska. The relatively carbon-poor and alkane-depleted sediments beneath
490 the lake phase might be a refrozen talik starting beneath the modern active layer (Unit III). ~~The brackish and refrozen sediments~~
491 ~~differed statistically from frozen upland deposits affected by freshwater conditions (Section 3.2.3). In Unit IV, increased TOC~~
492 ~~contents and a high *n*-alkane ratio, indicating the presence of herbaceous plants (Schäfer et al., 2016), point toward in Unit~~
493 ~~IV indicate one or even two wetland periods with organic matter accumulation, which likely occurred during the Holocene~~
494 ~~Thermal Maximum (Jones and Yu, 2010; Kaufman et al., 2004). The low TOC and TN content at 93 cm depth make it difficult~~
495 ~~to clarify whether a first wetland period was followed by another, as this impression could also result from cryoturbation. The~~
496 ~~age-depth inversion is an indication of both a refrozen talik and intensified freeze-thaw dynamics during the early Holocene.~~
497 Unit V represents the late Pleistocene to early Holocene transition as indicated by the trend towards ~~more negative higher~~ $\delta^{13}\text{C}$
498 values (Fig. 2d). ~~Brackish refrozen sediment could thereby be statistically distinguished from frozen upland deposits affected~~
499 ~~by freshwater conditions (Section 3.2.3).~~

500 4.1.4 Lagoons

501 If ~~thermokarst lakes or their~~ drained basins ~~or lakes~~ are connected and inundated by sea water, they become thermokarst
502 lagoons. With a size of 80 ha, the semi-open ~~thermokarst~~ lagoon is a relatively small ~~thermokarst~~ lagoon based on the circum-
503 Arctic thermokarst lagoon assessment published by Jenrich et al. (2025b). TOC contents are higher compared to other lagoons,
504 such as on the Bykovsky Peninsula in Siberia (Jenrich et al., 2021; Schirrmeister et al., 2018; Ulyantsev et al., 2017; Yang et
505 al., 2023), in northwestern Canada (Jenrich et al., 2025a), and the Teshepuk Lake area (Giest et al., 2025). Shoreline erosion
506 and fluvial organic matter input from streams (Fig. 1) are likely driving factors for this pattern.

507 Elson Lagoon, which is not a thermokarst lagoon, receives terrestrial sediment input through coastal erosion, and deposition
508 takes place as the barrier islands protect the waters of the lagoon (Brown et al., 2003; Ping et al., 2011; Zimmermann et al.,
509 2022). Our investigations indicate that the upper 80 cm of the sediments are terrestrial deposits, since the biogeochemical
510 parameters are overall very similar to the values found in the sediments of the thermokarst lagoon (Unit I; Fig. 2f, 3f). These
511 are underlain by likely late Pleistocene to early Holocene sandy sediments (Unit II).

512 The age-depth inversions signalize sediment mixing in both lagoons, which is favored through the semi- to unfrozen conditions
513 (Table S1). The hypersalinity in the sediments might be the result from concentrating salt through bedfasting ice in the shallow
514 lagoons (Jenrich et al., 2021). Hypersaline conditions in Elson Lagoon were quantified earlier by Osterkamp and Harrison
515 (1985) as well as Overduin et al. (2012).

516 4.2 Organic matter degradation patterns

517 For the terrestrial sampling measurements in the permafrost upland, the average C:N ratio (17.1 ± 2.1) compares well to values
518 reported in similar sites in northern Alaska (Fuchs et al., 2019; Giest et al., 2025; Ping et al., 2011). The comparably lower
519 ratio in the second meter (Unit V, VI) points towards a slightly higher degradation state (Fig. 2a). C:N ratios are lower
520 compared to permafrost-affected peat (20-60; Andersson et al., 2012) but similar or higher than in Yedoma deposits (9-19;
521 Strauss et al., 2022). Since $\delta^{13}\text{C}$ values become lighter (less negative) with degradation, C:N should correlate negatively with
522 $\delta^{13}\text{C}$ (Strauss et al., 2015). In our upland core however, this relationship shows a significant positive correlation (Fig. S1).
523 Since the CPI shows mixed but high (> 10) values, we can conclude that organic matter is overall relatively well preserved in
524 the upland. PERMANOVA test results indicated that frozen sediments are distinct from sediments affected by thaw processes,
525 namely unfrozen, refrozen and lagoon sediments. This expresses the possibility of statistically distinguishing between
526 sediments of various thaw histories.

527 For the first degradation stages with the subaquatic talik/cryopeg lake phase, PERMANOVA testing also revealed a distinct
528 biochemical signal of unfrozen sediments when compared to frozen, refrozen, and lagoon sediments. This result, as for the
529 upland, is likely influenced by source signals, especially when terrestrial and marine deposits are compared. But since the CPI
530 in the lakes (average 6.4) is comparably lower than in the upland (average 15.1) and the DLB (average 22.3), the organic
531 matter generally seems to be more degraded in the thermokarst lakes (Fig. 3). Moreover, the CPI in the saline East Twin Lake
532 sediments expressed signs for a stronger degradation signal (6.2) than in the brackish West Twin Lake sediments (6.9). This
533 might result from degradation under unfrozen cryotic, and saline conditions (Li et al., 2024). Compared to Yedoma and other
534 thermokarst lake sediments, the CPI values indicate a similar degree of organic matter decomposition (Jongejans et al., 2020)
535 or even stronger decomposition (Jongejans et al., 2021). In comparison to Yedoma and other thermokarst lake sediments, the
536 CPI indicates similar (Jongejans et al., 2020) to stronger (Jongejans et al., 2021) organic matter decomposition.

537 For the DLB, the carbon quality shows fresh organic matter in the surface peat (Unit I) which, together with the surface
538 sediments of the upland, makes seasonally frozen organic-rich sediments distinguishable from all other thermal regimes
539 considering C:N as shown by the Mann-Whitney tests (Fig. 4b). This is followed by more degraded conditions in the refrozen

540 talik ~~sediments~~ (Unit II, III) and well-preserved organic ~~matter earbon~~ in the former wetland phase (Unit IV). The C:N ratio
541 and the CPI index agree in their patterns; however, $\delta^{13}\text{C}$ only poorly reflects this picture (Fig. 2d, 3d). Therefore, C:N and
542 $\delta^{13}\text{C}$ resulted in a weak and ~~notnear~~-significant correlation. Especially the peak $\delta^{13}\text{C}$ values (least negative) in Unit I and IV
543 disturb the relationship, and it is likely that the source (i.e., lacustrine) signal of the isotopes is responsible for this pattern.
544 ~~Based on the C:N and CPI~~, Unit V indicates comparably stronger degraded organic matter ~~with an average C:N of 13.7 and a~~
545 ~~CPI of 12.5~~, combined with a marine $\delta^{13}\text{C}$ signal (maximum -25.0 ‰). The unique pattern of refrozen sediments is reflected
546 in the PERMANOVA results as the *refrozen* sediments could be differentiated from *frozen* and *unfrozen* terrestrial sediments
547 as well as *lagoon* deposits. Our DLB surface C:N and $\delta^{13}\text{C}$ values fit into the range observed by Wolter et al. (2024). Comparing
548 the average C:N of the full core (18.6~~±5.1~~) to other study areas in northern Alaska and northwest Canada however indicates
549 less degraded conditions than observed by Giest et al. (2025) (17.5), Fuchs et al. (2019) (16.6) and Wolter et al. (2017) (13.2).
550 The increased C:N ratios from Unit IV are pivotal reasons for this result, as early wetland phases were not described in the
551 aforementioned studies.

552 For the lagoons, the organic ~~matter earbon~~-degradation proxies reflect relatively little variability within the sediments and
553 represent a mixed signal from the terrestrial and lacustrine sites (Fig. 2, 3, 4). Although individual statistical tests of hypersaline
554 lagoon sediments revealed differences to other sediment types (section 3.2.1 and 3.2.2), the combined effect of thermal and
555 salinity regimes in lagoon sediments did not differ significantly from other sediment types (section 3.2.3). The reasons for this
556 are the various sediment types that are mixed in the investigated lagoons. The C:N ratio and CPI indicate relatively stronger
557 degraded material in the semi-open ~~thermokarst~~ lagoon compared to Elson Lagoon, though compared to lagoons in northern
558 Alaska and Siberia, both exhibit well-preserved organic ~~matter earbon~~, which can be explained by their terrestrial origin (Giest
559 et al., 2025; Jenrich et al., 2021; Schirmermeister et al., 2018; Yang et al., 2023).

560 4.3 Implications and outlook

561 Our biogeochemical investigations into representative landforms of northernmost coastal Alaska provide a valuable basis for
562 evaluating potential implications and future developments of the region. Based on this, we drew a conceptual model of
563 landscape dynamics in the study area (Fig. 6).

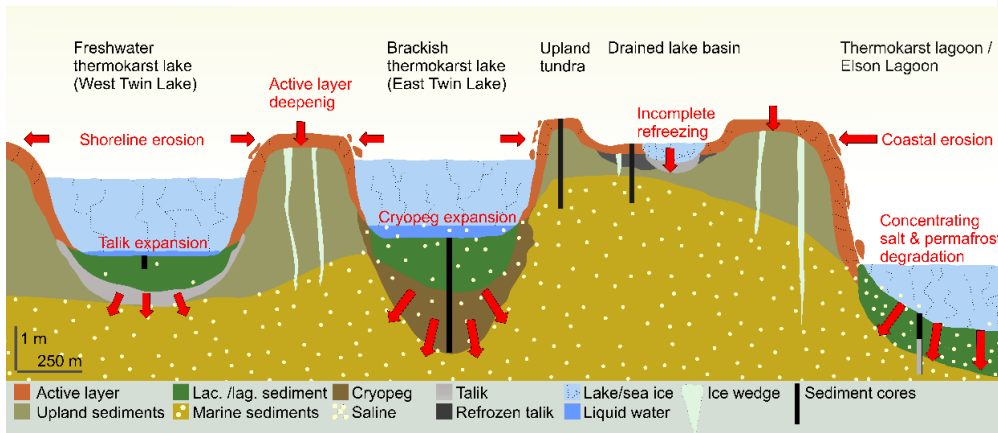


Figure 6: Conceptual illustration of physical properties and dynamics currently affecting the Utqiagvik Barrow Peninsula with potential for future acceleration. The sediments are present in a variety of thermal states, seasonally frozen (active layer), perennially frozen (upland tundra and subsea marine sediments), unfrozen (talik, lacustrine sediments, partly in the drained lake basin), unfrozen cryotic (cryopeg and lacustrine/lagoon sediments) and refrozen (drained lake basin). Model illustrated at approximate scale.

hat formatiert: Schriftfarbe: Automatisch

Remnant permafrost uplands cover ca. 28 % of today's landscape in the study area (Hinkel et al., 2005; Jones et al., 2022) where and saline permafrost underlays Holocene deposits (Brigham-Grette and Hopkins, 1995; Brouckov, 2003; Eisner et al., 2005). These non-saline sediments have a thickness of less than 1.5 m in our investigated upland. Increasing active layer depths in the tundra, with widespread thickening across >80 % of northern permafrost regions since 2003 (Liu et al., 2024; Smith et al., 2022) increasing active layer depths in the tundra (Liu et al., 2024; Smith et al., 2022) cause the mobilization and (dominantly) aerobic mineralization of organic carbon, leading to CO₂ production (Jenrich et al., 2024). Once thaw reaches to depths of the saline deposits, degradation processes will be enhanced as the freezing point is depressed. This poses the risk that subaerial taliks and cryopegs will be initiated earlier than -the 22nd century as hitherto projected by Parazoo et al. (2018). East Twin Lake has already undergone this development turning it from a freshwater to a brackish/saline thermokarst lake, which led to increased thermoerosion rates (Jones et al., 2023). Brown et al. (2003) calculated that the lake will likely drain into Elson Lagoon (or turn into a thermokarst lagoon) by the 2040s. However, this estimate was purely based on lake and lagoonal shoreline erosion rates while other processes, such as sea level rise, widespread gradual thaw with continued warming and rapid saline permafrost degradation were not accounted for (Creel et al., 2024; Guimond et al., 2021; Jones et al., 2023). These processes further increase the forcing, potentially leading to faster-than-anticipated landscape changes. The timing of a potential future drainage event of West Twin Lake is more difficult to estimate, but the drainage pathway may be via the thermoerosional gully to the south of the lake (Fig. 1). A supra-permafrost groundwater connection between the lake and Elson Lagoon may also play a (future) role in groundwater discharge (Dimova et al., 2015; Rawlins, 2021), yet Guimond et al. (2022)

587 conclude that groundwater is not a significant factor at the north Alaskan coast due to a low land to sea hydraulic gradient. The
588 talik beneath West Twin Lake has already reached brackish deposits, and with continued thaw beneath the lake, it can be
589 expected that the lake's water will turn brackish in the near future, too. This in turn would have implications for lake ice
590 dynamics and continued thaw beneath the lake. Arp et al. (2012) observed a trend from bedfast towards floating lake ice
591 conditions in northernmost Alaska, but the impact of saline conditions was not accounted for. Considering the vulnerability of
592 permafrost to salt, it can be expected that the aforementioned cascading effects of salt intrusion into lake waters will play a
593 crucial role across the Younger Outer Coastal Plain, as exemplified by East Twin Lake which has regionally representative
594 lake morphometrics (Table S1; Arp et al., 2011; Jones et al., 2023). The organic deposits within both lake's sediments are
595 already relatively stronger degraded than in the upland, and ~~organic matter carbon~~ of the cryopeg in East Twin Lake is more
596 heavily degraded than ~~carbon~~ in the West Twin Lake talik. From a microbiological point of view, this can be explained by
597 microbial communities that are likely dominated by methanogens (CH₄ producers) in West Twin Lake while in East Twin
598 Lake sulfate-reducing microbes (CO₂ producers) probably established additionally due to the saline deposits (Jenrich et al.,
599 2024; Yang et al., 2023). A potential co-existence of these microbial communities may lead to enhanced greenhouse gas
600 production (Jenrich et al., 2024; Yang et al., 2023). This comparison stresses the potential for year-round ~~saline salinity~~
601 ~~influenced organic carbon mineralization degradation~~ at sub-zero temperatures.

602 Northernmost Alaska is a highly dynamic region which is experiencing a net thermokarst lake area loss trend mostly due to
603 drainage of large lakes (Nitze et al., 2017; Webb et al., 2022). A detailed analysis of pond dynamics within DLBs on the
604 ~~Utqiagvik Barrow~~ Peninsula could also verify a drainage trend (Andresen and Lougheed, 2015). We investigated a wet but
605 terrestrial site within the DLB with a refrozen talik. Still, two larger thermokarst ponds are situated nearby with potential taliks
606 beneath. Thus, although the basin sequesters peat, it can be expected that ~~organic matter carbon~~ degradation also takes place
607 locally. Especially the former wetland phase (Unit IV, Fig. 2d, 3d) indicates well preserved organics ~~matter~~ in the sediment,
608 holding a high potential for ~~carbon~~ degradation. If these ponds drain, it can be expected that permafrost aggradation will
609 progressively slow with continued climate warming ~~and freezing point depression in saline deposits~~ (Jones et al., 2022; Lantz
610 et al., 2022). Moreover, Wolter et al. (2024) quantified high CH₄ concentrations in submerged areas within DLBs showcasing
611 the potential for carbon ~~mineralization degradation~~ under current environmental and climatic conditions.

612 When terrestrial or lacustrine deposits transition into, or are eroded into, lagoon systems, thawed organic ~~matter carbon~~
613 becomes vulnerable to decomposition under now hypersaline conditions. We found that the lagoonal deposits represent a
614 mixed signal of the terrestrial and lacustrine sediments rather than further advanced ~~carbon~~ degradation. With increasing
615 marine influence, it can be expected that greenhouse gas production shifts from mixed CH₄ and CO₂ in low connected water
616 bodies (such as the semi-open ~~thermokarst~~ lagoon) towards pure CO₂ production in more marine settings (like Elson Lagoon,
617 Jenrich et al., 2025a). Submarine permafrost degradation rates of up to 4 cm ~~yr⁻¹ per year~~ in Elson Lagoon (Overduin et al.,
618 2012) also contribute to enlarging the carbon pool ~~availability reactivity~~ for mineralization. The high ~~carbon~~ content ~~of TOC~~
619 and ~~the its~~ relatively well-preserved ~~organic matter state~~ therefore exhibits a large potential for future carbon mineralization in
620 lagoon systems.

hat formatiert: Hochgestellt

621 Overall, observed carbon and landscape dynamics can be expected to play a major role across the wider saline permafrost
622 region. Brouchkov (2003) published an estimated map of the saline permafrost zone, however large-scale quantifications of
623 the saline permafrost distribution and its properties, including organic carbon stocks, are currently lacking. This calls for future
624 study efforts, which would constitute important steps forward in understanding the role of salt in Arctic permafrost.

625 5. Conclusions

626 Our study reveals distinct patterns of organic ~~matter carbon~~ alteration along gradients of thaw and salinity stages ~~on in~~ the
627 Arctic ~~Ce~~oastal ~~Plain of Alaska~~lowland.

628 Regarding research question 1, which addressed how paleoenvironmental and modern processes shape present-day sediment
629 characteristics on the ~~Utqiagvik Barrow~~ Peninsula, we found that ~~late Pleistocene Late Glacial~~ saline deposits are overlain by
630 less than 1.5 m organic-rich, well-preserved sediments from an early Holocene wetland phase and a mid-Holocene active layer,
631 as observed in the DLB and the remnant permafrost upland, respectively. Thermokarst lake subsidence has transformed these
632 landscapes, with West Twin Lake reaching brackish sediment conditions and East Twin Lake progressing towards
633 brackish/saline states. Biogeochemical signatures indicate ongoing input of terrestrial and lacustrine sediments into the
634 lagoons.

635 In response to research question 2, which focused on organic matter quality in thermokarst landforms, we conclude that organic
636 ~~matter carbon~~ degradation is enhanced in the brackish talik of West Twin Lake and particularly in the cryopeg of East Twin
637 Lake. Lagoonal sediments show a high potential for carbon mineralization, driven by salt accumulation beneath bedfast ice
638 that has created hypersaline conditions. These conditions have maintained year-round unfrozen zones, enabling microbial
639 activity and greenhouse gas production.

640 Concerning research question 3, which asked how landscape dynamics affect organic matter mobilization, we anticipate that
641 deepening active layers, the formation of taliks and cryopegs, and ongoing shoreline erosion in lakes and lagoons will increase
642 the risk of organic carbon mobilization and mineralization. This risk is especially pronounced in saline deposits and may
643 accelerate landscape change across the saline permafrost region, with substantial implications for permafrost carbon release.

644 Our findings show a need for additional local investigations and upscaling efforts assessing the consequences of saline
645 permafrost thaw. While focused on a specific site on the northernmost tip of the USA, our study captures processes and
646 conditions that are likely characteristic of extensive saline permafrost landscapes across the Arctic, underscoring its
647 significance for regional-scale assessments of carbon dynamics.

648

649 Data availability

650

651 The data used for this study is available in the PANGAEA open access archive under:
652 <https://doi.pangaea.de/10.1594/PANGAEA.983965> (biogeochemical and hydrochemical data) and
653 <https://doi.pangaea.de/10.1594/PANGAEA.983966> (*n*-alkane data).

654

655 **Author Contributions**

656

657 FS and JS designed the study. JS, GG, MJ, and BMJ conducted fieldwork. FS, MJ, and JS carried out sediment subsampling.
658 FS conducted laboratory work, analyzed and plotted data, and wrote the first manuscript. All authors contributed to the
659 development of the paper.

660

661 **Competing interests**

662

663 Some authors are members of the editorial board of EGU Biogeosciences.

664

665 **Acknowledgements**

666

667 The SIPRE corer for this work was gratefully provided by Kenneth M. Hinkel (University of Cincinnati) and the vibracorer
668 was gratefully provided by Chris Mayo ([University of Alaska FairbanksUAF](#)). We also thank the Ukpeaġvik Iñupiat
669 Corporation (UIC) for issuing the permit for this research and providing logistical support. We would like to thank [Lars Ebel](#)
670 [and](#) the AWI laboratories Permafrost Biogeochemistry, Permafrost Hydrochemistry, ISOLAB and MICADAS for their
671 support. [Finally, we would like to thank the anonymous reviewers and the associate editor for their valuable comments.](#) This
672 work is a contribution to the IPA Saline Permafrost Action Group.

673

674 **Financial support**

675

676 FS and MJ received funding from the German Federal Environmental Foundation (Deutsche Bundesstiftung Umwelt).
677 Fieldwork was supported by NSF [Office of Polar Program awards -grants-](#)(1806213, 2336164) and AWI expedition baseline
678 funding. [The authors acknowledge support by the Open Access publication fund of Alfred Wegener Institute Helmholtz Centre](#)
679 [for Polar and Marine Research.](#)

680 **References**

681 Alewell, C., Giesler, R., Klaminder, J., Leifeld, J., and Rollog, M.: Stable carbon isotopes as indicators for environmental
682 change in peatlands, *Biogeosciences*, 8, 1769–1778, <https://doi.org/10.5194/bg-8-1769-2011>, 2011.

683 Andersson, R. A. and Meyers, P. A.: Effect of climate change on delivery and degradation of lipid biomarkers in a Holocene
684 peat sequence in the Eastern European Russian Arctic, *Organic Geochemistry*, 53, 63–72,
685 <https://doi.org/10.1016/j.orggeochem.2012.05.002>, 2012.

686 Andersson, R. A., Meyers, P., Hornibrook, E., Kuhry, P., and Mörth, C.-M.: Elemental and isotopic carbon and nitrogen
687 records of organic matter accumulation in a Holocene permafrost peat sequence in the East European Russian Arctic, *Journal*
688 *of Quaternary Science*, 27, 545–552, <https://doi.org/10.1002/jqs.2541>, 2012.

689 Andresen, C. G. and Lougheed, V. L.: Disappearing Arctic tundra ponds: Fine-scale analysis of surface hydrology in drained
690 thaw lake basins over a 65 year period (1948–2013), *J. Geophys. Res. Biogeosci.*, 120, 466–479,
691 <https://doi.org/10.1002/2014JG002778>, 2015.

692 Arp, C. D., Jones, B. M., Schmutz, J. A., Urban, F. E., and Jorgenson, M. T.: Two mechanisms of aquatic and terrestrial habitat
693 change along an Alaskan Arctic coastline, *Polar Biol*, 33, 1629–1640, <https://doi.org/10.1007/s00300-010-0800-5>, 2010.

694 Arp, C. D., Jones, B. M., Urban, F. E., and Grosse, G.: Hydrogeomorphic processes of thermokarst lakes with grounded-ice
695 and floating-ice regimes on the Arctic coastal plain, Alaska, *Hydrological Processes*, 25, 2422–2438,
696 <https://doi.org/10.1002/hyp.8019>, 2011.

697 Arp, C. D., Jones, B. M., Lu, Z., and Whitman, M. S.: Shifting balance of thermokarst lake ice regimes across the Arctic
698 Coastal Plain of northern Alaska, *Geophysical Research Letters*, 39, <https://doi.org/10.1029/2012GL052518>, 2012.

699 Athy, L. F.: Density, Porosity, and Compaction of Sedimentary Rocks¹, *AAPG Bulletin*, 14, 1–24,
700 <https://doi.org/10.1306/3D93289E-16B1-11D7-8645000102C1865D>, 1930.

701 Baas, M., Pancost, R., van Geel, B., and Sinninghe Damsté, J. S.: A comparative study of lipids in *Sphagnum* species, *Organic*
702 *Geochemistry*, 31, 535–541, [https://doi.org/10.1016/S0146-6380\(00\)00037-1](https://doi.org/10.1016/S0146-6380(00)00037-1), 2000.

703 Biskaborn, B. K., Smith, S. L., Noetzi, J., Matthes, H., Vieira, G., Streletskiy, D. A., Schoeneich, P., Romanovsky, V. E.,
704 Lewkowicz, A. G., Abramov, A., Allard, M., Boike, J., Cable, W. L., Christiansen, H. H., Delaloye, R., Diekmann, B.,
705 Drozdov, D., Etzelmüller, B., Grosse, G., Guglielmin, M., Ingeman-Nielsen, T., Isaksen, K., Ishikawa, M., Johansson, M.,
706 Johannsson, H., Joo, A., Kaverin, D., Kholodov, A., Konstantinov, P., Kröger, T., Lambiel, C., Lanckman, J.-P., Luo, D.,
707 Malkova, G., Meiklejohn, I., Moskalenko, N., Oliva, M., Phillips, M., Ramos, M., Sannel, A. B. K., Sergeev, D., Seybold, C.,
708 Skryabin, P., Vasiliev, A., Wu, Q., Yoshikawa, K., Zheleznyak, M., and Lantuit, H.: Permafrost is warming at a global scale,
709 *Nat Commun*, 10, 264, <https://doi.org/10.1038/s41467-018-08240-4>, 2019.

710 Black, R. F.: *Gubik Formation of Quaternary Age in Northern Alaska*, 302nd–C ed., U.S. Government Printing Office, 59–91
711 pp., 1964.

712 Blott, S. J. and Pye, K.: GRADISTAT: a grain size distribution and statistics package for the analysis of unconsolidated
713 sediments, *Earth Surface Processes and Landforms*, 26, 1237–1248, <https://doi.org/10.1002/esp.261>, 2001.

714 Bockheim, J. G., Everett, L. R., Hinkel, K. M., Nelson, F. E., and Brown, J.: Soil Organic Carbon Storage and Distribution in
715 Arctic Tundra, Barrow, Alaska, *Soil Science Society of America Journal*, 63, 934–940,
716 <https://doi.org/10.2136/sssaj1999.634934x>, 1999.

717 Bockheim, J. G., Hinkel, K. M., Eisner, W. R., and Dai, X. Y.: Carbon Pools and Accumulation Rates in an Age-Series of
718 Soils in Drained Thaw-Lake Basins, Arctic Alaska, *Soil Science Society of America Journal*, 68, 697–704,
719 <https://doi.org/10.2136/sssaj2004.6970>, 2004.

720 Bray, E. E. and Evans, E. D.: Hydrocarbons in Non-Reservoir-Rock Source Beds, *AAPG Bulletin*, 49, 248–257, 1965.

721 Brigham-Grette, J. and Hopkins, D. M.: Emergent Marine Record and Paleoclimate of the Last Interglaciation along the
722 Northwest Alaskan Coast, *Quaternary Research*, 43, 159–173, <https://doi.org/10.1006/qres.1995.1017>, 1995.

- 723 Brittingham, A., Hren, M. T., and Hartman, G.: Microbial alteration of the hydrogen and carbon isotopic composition of n-
724 alkanes in sediments, *Organic Geochemistry*, 107, 1–8, <https://doi.org/10.1016/j.orggeochem.2017.01.010>, 2017.
- 725 Brouchkov, A.: Nature and distribution of frozen saline sediments on the Russian Arctic coast, *Permafrost and Periglacial
726 Processes*, 13, 83–90, <https://doi.org/10.1002/ppp.411>, 2002.
- 727 Brouchkov, A.: Frozen saline soils of the Arctic coast: their distribution and engineering properties, *Proceedings of the eighth
728 international conference on permafrost*, 95–100, 2003.
- 729 Brown, J., Jorgenson, M. T., Smith, O. P., and Lee, W.: Long-term rates of coastal erosion and carbon input, Elson Lagoon,
730 Barrow, Alaska, *Proceedings of the 8th International Conference on Permafrost*, 101–106, 2003.
- 731 Cahyadi, A., Fatchurohman, H., and Riyanto, I. A.: Groundwater quality analysis in dry seasons in Panggang Cay, Kepulauan
732 Seribu, Jakarta, Indonesia, *IOP Conf. Ser.: Earth Environ. Sci.*, 212, 012001, <https://doi.org/10.1088/1755-1315/212/1/012001>,
733 2018.
- 734 Carter, L. D.: A Pleistocene Sand Sea on the Alaskan Arctic Coastal Plain, *Science*, 211, 381–383,
735 <https://doi.org/10.1126/science.211.4480.381>, 1981.
- 736 Chen, Y., Lara, M. J., Jones, B. M., Frost, G. V., and Hu, F. S.: Thermokarst acceleration in Arctic tundra driven by climate
737 change and fire disturbance, *One Earth*, 4, 1718–1729, <https://doi.org/10.1016/j.oneear.2021.11.011>, 2021.
- 738 Chylek, P., Folland, C., Klett, J. D., Wang, M., Hengartner, N., Lesins, G., and Dubey, M. K.: Annual Mean Arctic
739 Amplification 1970–2020: Observed and Simulated by CMIP6 Climate Models, *Geophysical Research Letters*, 49,
740 e2022GL099371, <https://doi.org/10.1029/2022GL099371>, 2022.
- 741 Copernicus: Copernicus Sentinel-2 (processed by ESA), MSI Level-2A BOA Reflectance Product. Collection 0. European
742 Space Agency, https://doi.org/10.5270/S2_-6eb6imz, 2023.
- 743 Coplen, T. B., Brand, W. A., Gehre, M., Gröning, M., Meijer, H. A. J., Toman, B., and Verkouteren, R. M.: New Guidelines
744 for $\delta^{13}\text{C}$ Measurements, *Anal. Chem.*, 78, 2439–2441, <https://doi.org/10.1021/ac052027c>, 2006.
- 745 Creel, R., Guimond, J., Jones, B. M., Nielsen, D. M., Bristol, E., Tweedie, C. E., and Overduin, P. P.: Permafrost thaw
746 subsidence, sea-level rise, and erosion are transforming Alaska’s Arctic coastal zone, *Proceedings of the National Academy
747 of Sciences*, 121, e2409411121, <https://doi.org/10.1073/pnas.2409411121>, 2024.
- 748 DGGs: DGGs Elevation Portal, 2018.
- 749 Diefendorf, A. F., Freeman, K. H., Wing, S. L., and Graham, H. V.: Production of n-alkyl lipids in living plants and
750 implications for the geologic past, *Geochimica et Cosmochimica Acta*, 75, 7472–7485,
751 <https://doi.org/10.1016/j.gca.2011.09.028>, 2011.
- 752 Dimova, N. T., Paytan, A., Kessler, J. D., Sparrow, K. J., Garcia-Tigreros Kodovska, F., Lecher, A. L., Murray, J., and
753 Tulaczyk, S. M.: Current Magnitude and Mechanisms of Groundwater Discharge in the Arctic: Case Study from Alaska,
754 *Environ. Sci. Technol.*, 49, 12036–12043, <https://doi.org/10.1021/acs.est.5b02215>, 2015.
- 755 Eglinton, G., Hamilton, R. J., Raphael, R. A., and Gonzalez, A. G.: Hydrocarbon Constituents of the Wax Coatings of Plant
756 Leaves: A Taxonomic Survey, *Nature*, 193, 739–742, <https://doi.org/10.1038/193739a0>, 1962.

- 757 Eisner, W. R., Bockheim, J. G., Hinkel, K. M., Brown, T. A., Nelson, F. E., Peterson, K. M., and Jones, B. M.:
 758 Paleoenvironmental analyses of an organic deposit from an erosional landscape remnant, Arctic Coastal Plain of Alaska,
 759 *Palaeogeography, Palaeoclimatology, Palaeoecology*, 217, 187–204, <https://doi.org/10.1016/j.palaeo.2004.11.025>, 2005.
- 760 van Everdingen, R. O. (Ed.): *Multi-language Glossary of Permafrost and Related Ground-ice Terms in Chinese, English,*
 761 *French, German, Icelandic, Italian, Norwegian, Polish, Romanian, Spanish, and Swedish*, Arctic Inst. of North America
 762 University of Calgary, Calgary, Alberta, Canada, 2005.
- 763 Farquharson, L. M., Romanovsky, V. E., Kholodov, A., and Nicolsky, D.: Sub-aerial talik formation observed across the
 764 discontinuous permafrost zone of Alaska, *Nat. Geosci.*, <https://doi.org/10.1038/s41561-022-00952-z>, 2022.
- 765 Ficken, K. J., Li, B., Swain, D. L., and Eglinton, G.: An n-alkane proxy for the sedimentary input of submerged/floating
 766 freshwater aquatic macrophytes, *Organic Geochemistry*, 31, 745–749, [https://doi.org/10.1016/S0146-6380\(00\)00081-4](https://doi.org/10.1016/S0146-6380(00)00081-4), 2000.
- 767 Fuchs, M., Lenz, J., Jock, S., Nitze, I., Jones, B. M., Strauss, J., Günther, F., and Grosse, G.: Organic Carbon and Nitrogen
 768 Stocks Along a Thermokarst Lake Sequence in Arctic Alaska, *Journal of Geophysical Research: Biogeosciences*, 124, 1230–
 769 1247, <https://doi.org/10.1029/2018JG004591>, 2019.
- 770 Gibbs, A. E. and Richmond, B. M.: National assessment of shoreline change—Summary statistics for updated vector shorelines
 771 and associated shoreline change data for the north coast of Alaska, U.S.- Canadian border to Icy Cape, U.S. Geological Survey,
 772 Virginia, US, 2017.
- 773 Giest, F. P., Jenrich, M., Grosse, G., Jones, B. M., Mangelsdorf, K., Windirsch, T., and Strauss, J.: Organic carbon, mercury,
 774 and sediment characteristics along a land–shore transect in Arctic Alaska, *Biogeosciences*, 22, 2871–2887,
 775 <https://doi.org/10.5194/bg-22-2871-2025>, 2025.
- 776 [Goñi, M. A., Yunker, M. B., MacDonald, R. W., and Eglinton, T. I.: Distribution and sources of organic biomarkers in Arctic
 777 sediments from the Mackenzie River and Beaufort Shelf, *Mar. Chem.*, 71, 23–51, \[https://doi.org/10.1016/S0304-
 778 4203\\(00\\)00037-2\]\(https://doi.org/10.1016/S0304-4203\(00\)00037-2\), 2000.](#)
- 779 Grosse, G., Harden, J., Turetsky, M., McGuire, A. D., Camill, P., Tarnocai, C., Frolking, S., Schuur, E. A. G., Jorgenson, T.,
 780 Marchenko, S., Romanovsky, V., Wickland, K. P., French, N., Waldrop, M., Bourgeau-Chavez, L., and Striegl, R. G.:
 781 Vulnerability of high-latitude soil organic carbon in North America to disturbance, *J. Geophys. Res.*, 116, G00K06,
 782 <https://doi.org/10.1029/2010JG001507>, 2011.
- 783 Guimond, J. A., Mohammed, A. A., Walvoord, M. A., Bense, V. F., and Kurylyk, B. L.: Saltwater Intrusion Intensifies Coastal
 784 Permafrost Thaw, *Geophysical Research Letters*, 48, e2021GL094776, <https://doi.org/10.1029/2021GL094776>, 2021.
- 785 Guimond, J. A., Mohammed, A. A., Walvoord, M. A., Bense, V. F., and Kurylyk, B. L.: Sea-level rise and warming mediate
 786 coastal groundwater discharge in the Arctic, *Environ. Res. Lett.*, 17, 045027, <https://doi.org/10.1088/1748-9326/ac6085>, 2022.
- 787 Harris, C. M., McClelland, J. W., Connelly, T. L., Crump, B. C., and Dunton, K. H.: Salinity and Temperature Regimes in
 788 Eastern Alaskan Beaufort Sea Lagoons in Relation to Source Water Contributions, *Estuaries and Coasts*, 40, 50–62,
 789 <https://doi.org/10.1007/s12237-016-0123-z>, 2017.
- 790 Haugk, C., Jongejans, L. L., Mangelsdorf, K., Fuchs, M., Ogneva, O., Palmtag, J., Mollenhauer, G., Mann, P. J., Overduin, P.
 791 P., Grosse, G., Sanders, T., Tuerena, R. E., Schirrmeister, L., Wetterich, S., Kizyakov, A., Karger, C., and Strauss, J.: Organic
 792 matter characteristics of a rapidly eroding permafrost cliff in NE Siberia (Lena Delta, Laptev Sea region), *Biogeosciences*, 19,
 793 2079–2094, <https://doi.org/10.5194/bg-19-2079-2022>, 2022.

hat formatiert: Schriftfarbe: Automatisch

hat formatiert: Schriftfarbe: Automatisch

794 Hinkel, K. M., Eisner, W. R., Bockheim, J. G., Nelson, F. E., Peterson, K. M., and Dai, X.: Spatial Extent, Age, and Carbon
795 Stocks in Drained Thaw Lake Basins on the Barrow Peninsula, Alaska, Arctic, Antarctic, and Alpine Research, 35, 291–300,
796 [https://doi.org/10.1657/1523-0430\(2003\)035%255B0291:SEAACS%255D2.0.CO;2](https://doi.org/10.1657/1523-0430(2003)035%255B0291:SEAACS%255D2.0.CO;2), 2003.

797 Hinkel, K. M., Frohn, R. C., Nelson, F. E., Eisner, W. R., and Beck, R. A.: Morphometric and spatial analysis of thaw lakes
798 and drained thaw lake basins in the western Arctic Coastal Plain, Alaska, Permafrost and Periglacial Processes, 16, 327–341,
799 <https://doi.org/10.1002/ppp.532>, 2005.

800 Irrgang, A. M., Bendixen, M., Farquharson, L. M., Baranskaya, A. V., Erikson, L. H., Gibbs, A. E., Ogorodov, S. A., Overduin,
801 P. P., Lantuit, H., Grigoriev, M. N., and Jones, B. M.: Drivers, dynamics and impacts of changing Arctic coasts, Nat Rev Earth
802 Environ, 3, 39–54, <https://doi.org/10.1038/s43017-021-00232-1>, 2022.

803 Jenrich, M., Angelopoulos, M., Grosse, G., Overduin, P. P., Schirrmeister, L., Nitze, I., Biskaborn, B. K., Liebner, S.,
804 Grigoriev, M., Murray, A., Jongejans, L. L., and Strauss, J.: Thermokarst lagoons: A core-based assessment of depositional
805 characteristics and an estimate of carbon pools on the Bykovsky Peninsula, Frontiers in Earth Science, 9, 2021.

806 Jenrich, M., Angelopoulos, M., Liebner, S., Treat, C., Knoblauch, C., Yang, S., Grosse, G., Giebeler, F., Jongejans, L. L.,
807 Grigoriev, M., and Strauss, J.: Greenhouse Gas Production and Microbial Response During the Transition From Terrestrial
808 Permafrost to a Marine Environment, Permafrost and Periglacial Processes, 36, 63–82, <https://doi.org/10.1002/ppp.2251>, 2024.

809 Jenrich, M., Wolter, J., Liebner, S., Knoblauch, C., Grosse, G., Giebeler, F., Whalen, D., and Strauss, J.: Rising Arctic seas
810 and thawing permafrost: uncovering the carbon cycle impact in a thermokarst lagoon system in the outer Mackenzie Delta,
811 Canada, Biogeosciences, 22, 2069–2086, <https://doi.org/10.5194/bg-22-2069-2025>, 2025a.

812 Jenrich, M., Proding, M., Nitze, I., Grosse, G., and Strauss, J.: Thermokarst Lagoons: Distribution, Classification and
813 Dynamics in Permafrost-to-Marine Transitions, Permafrost and Periglacial Processes, n/a, <https://doi.org/10.1002/ppp.70001>,
814 2025b.

815 Jones, B. M., Arp, C. D., Grosse, G., Nitze, I., Lara, M. J., Whitman, M. S., Farquharson, L. M., Kanevskiy, M., Parsekian, A.
816 D., Breen, A. L., Ohara, N., Rangel, R. C., and Hinkel, K. M.: Identifying historical and future potential lake drainage events
817 on the western Arctic coastal plain of Alaska, Permafrost and Periglacial Process, 31, 110–127, <https://doi.org/10.1002/ppp.2038>,
818 2020.

819 Jones, B. M., Grosse, G., Farquharson, L. M., Roy-Léveillé, P., Veremeeva, A., Kanevskiy, M. Z., Gaglioti, B. V., Breen, A.
820 L., Parsekian, A. D., Ulrich, M., and Hinkel, K. M.: Lake and drained lake basin systems in lowland permafrost regions, Nat
821 Rev Earth Environ, 3, 85–98, <https://doi.org/10.1038/s43017-021-00238-9>, 2022.

822 Jones, B. M., Kanevskiy, M. Z., Parsekian, A. D., Bergstedt, H., Ward Jones, M. K., Rangel, R. C., Hinkel, K. M., and Shur,
823 Y.: Rapid Saline Permafrost Thaw Below a Shallow Thermokarst Lake in Arctic Alaska, Geophysical Research Letters, 50,
824 e2023GL105552, <https://doi.org/10.1029/2023GL105552>, 2023.

825 Jones, M. C. and Yu, Z.: Rapid deglacial and early Holocene expansion of peatlands in Alaska, Proceedings of the National
826 Academy of Sciences, 107, 7347–7352, <https://doi.org/10.1073/pnas.0911387107>, 2010.

827 Jones, M. C., Grosse, G., Jones, B. M., and Walter Anthony, K. M.: Peat accumulation in drained thermokarst lake basins in
828 continuous, ice-rich permafrost, northern Seward Peninsula, Alaska, J. Geophys. Res., 117,
829 <https://doi.org/10.1029/2011JG001766>, 2012.

- 830 Jong, D., Bröder, L., Tesi, T., Tanski, G., Oudenhuisen, M., Fritz, M., Lantuit, H., Haghypour, N., Eglinton, T., and Vonk, J.:
 831 Selective Sorting and Degradation of Permafrost Organic Matter in the Nearshore Zone of Herschel Island (Yukon, Canada),
 832 *Journal of Geophysical Research: Biogeosciences*, 129, e2023JG007479, <https://doi.org/10.1029/2023JG007479>, 2024.
- 833 Jongejans, L. L., Mangelsdorf, K., Schirrmeister, L., Grigoriev, M. N., Maksimov, G. M., Biskaborn, B. K., Grosse, G., and
 834 Strauss, J.: n-Alkane Characteristics of Thawed Permafrost Deposits Below a Thermokarst Lake on Bykovsky Peninsula,
 835 Northeastern Siberia, *Front. Environ. Sci.*, 8, 118, <https://doi.org/10.3389/fenvs.2020.00118>, 2020.
- 836 Jongejans, L. L., Liebner, S., Knoblauch, C., Mangelsdorf, K., Ulrich, M., Grosse, G., Tanski, G., Fedorov, A. N.,
 837 Konstantinov, P. Ya., Windirsch, T., Wiedmann, J., and Strauss, J.: Greenhouse gas production and lipid biomarker distributio
 838 in Yedoma and Alas thermokarst lake sediments in Eastern Siberia, *Global Change Biology*, 27, 2822–2839,
 839 <https://doi.org/10.1111/gcb.15566>, 2021.
- 840 Kaufman, D. S., Ager, T. A., Anderson, N. J., Anderson, P. M., Andrews, J. T., Bartlein, P. J., Brubaker, L. B., Coats, L. L.,
 841 Cwynar, L. C., Duvall, M. L., Dyke, A. S., Edwards, M. E., Eisner, W. R., Gajewski, K., Geirsdóttir, A., Hu, F. S., Jennings,
 842 A. E., Kaplan, M. R., Kerwin, M. W., Lozhkin, A. V., MacDonald, G. M., Miller, G. H., Mock, C. J., Oswald, W. W., Otto-
 843 Bliesner, B. L., Porinchu, D. F., Rühland, K., Smol, J. P., Steig, E. J., and Wolfe, B. B.: Holocene thermal maximum in the
 844 western Arctic (0–180°W), *Quaternary Science Reviews*, 23, 529–560, <https://doi.org/10.1016/j.quascirev.2003.09.007>, 2004.
- 845 Killips, S. D. and Killips, V. J.: *Introduction to organic geochemistry*, 2nd ed., Blackwell Pub, Malden, MA, 393 pp., 2005.
- 846 [Lantz, T. C., Zhang, Y., and Kokelj, S. V.: Impacts of ecological succession and climate warming on permafrost aggradation
 847 in drained lake basins of the Tuktoyaktuk Coastlands, Northwest Territories, Canada, *Permafrost & Periglacial*, 33, 176–192,
 848 <https://doi.org/10.1002/ppp.2143>, 2022.](https://doi.org/10.1002/ppp.2143)
- 849 Lara, M. J., McGuire, A. D., Euskirchen, E. S., Tweedie, C. E., Hinkel, K. M., Skurikhin, A. N., Romanovsky, V. E., Grosse,
 850 G., Bolton, W. R., and Genet, H.: Polygonal tundra geomorphological change in response to warming alters future CO₂ and
 851 CH₄ flux on the Barrow Peninsula, *Global Change Biology*, 21, 1634–1651, <https://doi.org/10.1111/gcb.12757>, 2015.
- 852 Lara, M. J., McGuire, A. D., Euskirchen, E. S., Genet, H., Yi, S., Rutter, R., Iversen, C., Sloan, V., and Wullschleger, S. D.:
 853 Local-scale Arctic tundra heterogeneity affects regional-scale carbon dynamics, *Nat Commun*, 11, 4925,
 854 <https://doi.org/10.1038/s41467-020-18768-z>, 2020.
- 855 Lara, M. J., Michaelides, R., Anderson, D., Chen, W., Hall, E. C., Ludden, C., Schore, A. I. G., Mishra, U., and Scott, S. N.:
 856 A 20 m spatial resolution peatland extent map of Alaska, *Sci Data*, 12, 226, <https://doi.org/10.1038/s41597-025-04502-1>, 2025.
- 857 Lenz, J., Jones, B. M., Wetterich, S., Tjallingii, R., Fritz, M., Arp, C. D., Rudaya, N., and Grosse, G.: Impacts of shore
 858 expansion and catchment characteristics on lacustrine thermokarst records in permafrost lowlands, Alaska Arctic Coastal Plain,
 859 *Arktos*, 2, 25, <https://doi.org/10.1007/s41063-016-0025-0>, 2016.
- 860 Li, M., Li, Z., Dong, S., Chen, L., Su, X., Lu, C., Zhou, A., and Wang, N.: Salinity impacts on n-alkanes in lake sediments of
 861 the Badain Jaran Desert, Northwestern China: Implications for paleoclimate reconstruction, *Palaeogeography,
 862 Palaeoclimatology, Palaeoecology*, 656, 112571, <https://doi.org/10.1016/j.palaeo.2024.112571>, 2024.
- 863 Ling, F. and Zhang, T.: Modeling study of talik freeze-up and permafrost response under drained thaw lakes on the Alaskan
 864 Arctic Coastal Plain, *Journal of Geophysical Research: Atmospheres*, 109, <https://doi.org/10.1029/2003JD003886>, 2004.
- 865 Lisiecki, L. E. and Herbert, T. D.: Automated composite depth scale construction and estimates of sediment core extension,
 866 *Paleoceanography*, 22, <https://doi.org/10.1029/2006PA001401>, 2007.

hat formatiert: Schriftfarbe: Schwarz

hat formatiert: Schriftfarbe: Automatisch

- 867 Liu, Z., Kimball, J. S., Ballantyne, A., Watts, J. D., Natali, S. M., Rogers, B. M., Yi, Y., Klene, A. E., Moghaddam, M., Du,
868 J., and Zona, D.: Widespread deepening of the active layer in northern permafrost regions from 2003 to 2020, *Environ. Res.*
869 *Let.*, 19, 014020, <https://doi.org/10.1088/1748-9326/ad0f73>, 2024.
- 870 Lougheed, V. L., Tweedie, C. E., Andresen, C. G., Armendariz, A. M., Escarzaga, S. M., and Tarin, G.: Patterns and Drivers
871 of Carbon Dioxide Concentrations in Aquatic Ecosystems of the Arctic Coastal Tundra, *Global Biogeochemical Cycles*, 34,
872 e2020GB006552, <https://doi.org/10.1029/2020GB006552>, 2020.
- 873 Maffei, M.: Chemotaxonomic significance of leaf wax alkanes in the gramineae, *Biochemical Systematics and Ecology*, 24,
874 53–64, [https://doi.org/10.1016/0305-1978\(95\)00102-6](https://doi.org/10.1016/0305-1978(95)00102-6), 1996.
- 875 [Martens, J., Mueller, C. W., Joshi, P., Rosinger, C., Maisch, M., Kappler, A., Bonkowski, M., Schwamborn, G., Schirrmeister,](#)
876 [L., and Rethemeyer, J.: Stabilization of mineral-associated organic carbon in Pleistocene permafrost, *Nature Communications*,](#)
877 [14, 2120, https://doi.org/10.1038/s41467-023-37766-5, 2023.](#)
- 878 Marzi, R., Torkelson, B. E., and Olson, R. K.: A revised carbon preference index, *Organic Geochemistry*, 20, 1303–1306,
879 [https://doi.org/10.1016/0146-6380\(93\)90016-5](https://doi.org/10.1016/0146-6380(93)90016-5), 1993.
- 880 McGuire, A. D., Koven, C., Lawrence, D. M., Clein, J. S., Xia, J., Beer, C., Burke, E., Chen, G., Chen, X., Delire, C., Jafarov,
881 E., MacDougall, A. H., Marchenko, S., Nicolsky, D., Peng, S., Rinke, A., Saito, K., Zhang, W., Alkama, R., Bohn, T. J., Ciais,
882 P., Decharme, B., Ekici, A., Gouttevin, I., Hajima, T., Hayes, D. J., Ji, D., Krinner, G., Lettenmaier, D. P., Luo, Y., Miller, P.
883 A., Moore, J. C., Romanovsky, V., Schädel, C., Schaefer, K., Schuur, E. A. G., Smith, B., Sueyoshi, T., and Zhuang, Q.:
884 Variability in the sensitivity among model simulations of permafrost and carbon dynamics in the permafrost region between
885 1960 and 2009, *Global Biogeochemical Cycles*, 30, 1015–1037, <https://doi.org/10.1002/2016GB005405>, 2016.
- 886 Meyer, H., Schirrmeister, L., Andreev, A., Wagner, D., Hubberten, H.-W., Yoshikawa, K., Bobrov, A., Wetterich, S., Opel,
887 T., Kandiano, E., and Brown, J.: Lateglacial and Holocene isotopic and environmental history of northern coastal Alaska –
888 Results from a buried ice-wedge system at Barrow, *Quaternary Science Reviews*, 29, 3720–3735,
889 <https://doi.org/10.1016/j.quascirev.2010.08.005>, 2010.
- 890 Meyers, P. A.: Preservation of elemental and isotopic source identification of sedimentary organic matter, *Chemical Geology*,
891 114, 289–302, [https://doi.org/10.1016/0009-2541\(94\)90059-0](https://doi.org/10.1016/0009-2541(94)90059-0), 1994.
- 892 Mollenhauer, G., Grotheer, H., Gentz, T., Bonk, E., and Hefter, J.: Standard operation procedures and performance of the
893 MICADAS radiocarbon laboratory at Alfred Wegener Institute (AWI), Germany, *Nuclear Instruments and Methods in Physics*
894 *Research Section B: Beam Interactions with Materials and Atoms*, 496, 45–51, <https://doi.org/10.1016/j.nimb.2021.03.016>,
895 2021.
- 896 Mu, M., Mu, C., Liu, H., Lei, P., Ge, Y., Zhou, Z., Peng, X., and Ma, T.: Thermokarst lake drainage halves the temperature
897 sensitivity of CH₄ release on the Qinghai-Tibet Plateau, *Nat Commun*, 16, 1992, [https://doi.org/10.1038/s41467-025-57356-](https://doi.org/10.1038/s41467-025-57356-x)
898 [x](#), 2025.
- 899 Nielsen, D. M., Pieper, P., Barkhordarian, A., Overduin, P., Ilyina, T., Brovkin, V., Baehr, J., and Dobrynin, M.: Increase in
900 Arctic coastal erosion and its sensitivity to warming in the twenty-first century, *Nat. Clim. Chang.*, 12, 263–270,
901 <https://doi.org/10.1038/s41558-022-01281-0>, 2022.
- 902 Nitzbon, J., Schneider von Deimling, T., Aliyeva, M., Chadburn, S. E., Grosse, G., Laboor, S., Lee, H., Lohmann, G., Steinert,
903 N. J., Stuenzi, S. M., Werner, M., Westermann, S., and Langer, M.: No respite from permafrost-thaw impacts in the absence
904 of a global tipping point, *Nat. Clim. Chang.*, 14, 573–585, <https://doi.org/10.1038/s41558-024-02011-4>, 2024.

hat formatiert: Schriftfarbe: Automatisch

hat formatiert: Schriftfarbe: Automatisch

905 Nitze, I., Grosse, G., Jones, B. M., Arp, C. D., Ulrich, M., Fedorov, A., and Veremeeva, A.: Landsat-Based Trend Analysis of
906 Lake Dynamics across Northern Permafrost Regions, *Remote Sensing*, 9, 640, <https://doi.org/10.3390/rs9070640>, 2017.

907 Nyland, K. E., Shiklomanov, N. I., Streletskiy, D. A., Nelson, F. E., Klene, A. E., and Kholodov, A. L.: Long-term Circumpolar
908 Active Layer Monitoring (CALM) program observations in Northern Alaskan tundra, *Polar Geography*, 44, 167–185,
909 <https://doi.org/10.1080/1088937X.2021.1988000>, 2021.

910 Obu, J., Westermann, S., Kääb, A., and Bartsch, A.: Ground Temperature Map, 2000–2016, Northern Hemisphere Permafrost,
911 <https://doi.org/10.1594/PANGAEA.888600>, 2018.

912 Obu, J., Westermann, S., Bartsch, A., Berdnikov, N., Christiansen, H. H., Dashtseren, A., Delaloye, R., Elberling, B.,
913 Etzelmüller, B., Kholodov, A., Khomutov, A., Kääb, A., Leibman, M. O., Lewkowicz, A. G., Panda, S. K., Romanovsky, V.,
914 Way, R. G., Westergaard-Nielsen, A., Wu, T., Yamkhin, J., and Zou, D.: Northern Hemisphere permafrost map based on
915 TTOP modelling for 2000–2016 at 1 km² scale, *Earth-Science Reviews*, 193, 299–316,
916 <https://doi.org/10.1016/j.earscirev.2019.04.023>, 2019.

917 Osterkamp, T. E.: Occurrence and potential importance of saline permafrost in Alaska, Workshop on Saline Permafrost, 1989.

918 Osterkamp, T. E. and Harrison, W. D.: Temperature measurements in subsea permafrost off the coast of Alaska, 4th Canadian
919 Permafrost Conf., 1982.

920 Osterkamp, T. E. and Harrison, W. D.: Subsea permafrost: Probing, thermal regime and data analysis, U.S. Dep. of Commer.,
921 NOAA, Environ. Res. Lab., Boulder, Colorado, US, 1985.

922 Otto, A. and Simpson, M. J.: Degradation and Preservation of Vascular Plant-derived Biomarkers in Grassland and Forest
923 Soils from Western Canada, *Biogeochemistry*, 74, 377–409, <https://doi.org/10.1007/s10533-004-5834-8>, 2005.

924 Overduin, P. P., Westermann, S., Yoshikawa, K., Haberlau, T., Romanovsky, V., and Wetterich, S.: Geoelectric observations
925 of the degradation of nearshore submarine permafrost at Barrow (Alaskan Beaufort Sea), *Journal of Geophysical Research: Earth Surface*, 117, <https://doi.org/10.1029/2011JF002088>, 2012.

927 Parazoo, N. C., Koven, C. D., Lawrence, D. M., Romanovsky, V., and Miller, C. E.: Detecting the permafrost carbon feedback:
928 talik formation and increased cold-season respiration as precursors to sink-to-source transitions, *The Cryosphere*, 12, 123–
929 144, <https://doi.org/10.5194/tc-12-123-2018>, 2018.

930 Ping, C.-L., Michaelson, G. J., Guo, L., Jorgenson, M. T., Kanevskiy, M., Shur, Y., Dou, F., and Liang, J.: Soil carbon and
931 material fluxes across the eroding Alaska Beaufort Sea coastline, *Journal of Geophysical Research: Biogeosciences*, 116,
932 <https://doi.org/10.1029/2010JG001588>, 2011.

933 Poynter, J. and Eglinton, G.: Molecular composition of three sediments from hole 717c: the Bengal fan, edited by: Cochran,
934 J. R., Stow, D. A. V., and et al., Ocean Drilling Program, <https://doi.org/10.2973/odp.proc.sr.116.1990>, 1990.

935 Radke, Matthias., Willsch, Helmut., and Welte, D. H.: Preparative hydrocarbon group type determination by automated
936 medium pressure liquid chromatography, *Anal. Chem.*, 52, 406–411, <https://doi.org/10.1021/ac50053a009>, 1980.

937 Rantanen, M., Karpechko, A. Y., Lipponen, A., Nordling, K., Hyvärinen, O., Ruosteenoja, K., Vihma, T., and Laaksonen, A.:
938 The Arctic has warmed nearly four times faster than the globe since 1979, *Commun Earth Environ*, 3, 1–10,
939 <https://doi.org/10.1038/s43247-022-00498-3>, 2022.

- 940 Rawlins, M. A.: Increasing freshwater and dissolved organic carbon flows to Northwest Alaska's Elson lagoon, *Environ. Res. Lett.*, 16, 105014, <https://doi.org/10.1088/1748-9326/ac2288>, 2021.
- 941
- 942 Reimer, P. J., Austin, W. E. N., Bard, E., Bayliss, A., Blackwell, P. G., Ramsey, C. B., Butzin, M., Cheng, H., Edwards, R. L.,
943 Friedrich, M., Grootes, P. M., Guilderson, T. P., Hajdas, I., Heaton, T. J., Hogg, A. G., Hughen, K. A., Kromer, B., Manning,
944 S. W., Muscheler, R., Palmer, J. G., Pearson, C., Plicht, J. van der, Reimer, R. W., Richards, D. A., Scott, E. M., Southon, J.
945 R., Turney, C. S. M., Wacker, L., Adolphi, F., Büntgen, U., Capano, M., Fahrni, S. M., Fogtmann-Schulz, A., Friedrich, R.,
946 Köhler, P., Kudsk, S., Miyake, F., Olsen, J., Reing, F., Sakamoto, M., Sookdeo, A., and Talamo, S.: The IntCal20 Northern
947 Hemisphere Radiocarbon Age Calibration Curve (0–55 cal kBP), *Radiocarbon*, 62, 725–757,
948 <https://doi.org/10.1017/RDC.2020.41>, 2020.
- 949 Schäfer, I. K., Lanny, V., Franke, J., Eglinton, T. I., Zech, M., Vysloužilová, B., and Zech, R.: Leaf waxes in litter and topsoils
950 along a European transect, *SOIL*, 2, 551–564, <https://doi.org/10.5194/soil-2-551-2016>, 2016.
- 951 Schirrmeister, L., Grigoriev, M. N., Strauss, J., Grosse, G., Overduin, P. P., Kholodov, A., Guenther, F., and Hubberten, H.-
952 W.: Sediment characteristics of a thermokarst lagoon in the northeastern Siberian Arctic (Ivashkina Lagoon, Bykovsky
953 Peninsula), *Arktos*, 4, 1–16, <https://doi.org/10.1007/s41063-018-0049-8>, 2018.
- 954 Schuur, E. A. G., Abbott, B. W., Commane, R., Ernakovich, J., Euskirchen, E., Hugelius, G., Grosse, G., Jones, M., Koven,
955 C., Leshyk, V., Lawrence, D., Lorant, M. M., Mauritz, M., Olefeldt, D., Natali, S., Rodenhizer, H., Salmon, V., Schädel, C.,
956 Strauss, J., Treat, C., and Turetsky, M.: Permafrost and Climate Change: Carbon Cycle Feedbacks From the Warming Arctic,
957 *Annual Review of Environment and Resources*, 47, 343–371, <https://doi.org/10.1146/annurev-environ-012220-011847>, 2022.
- 958 Schwamborn, G., Schirrmeister, L., Mohammadi, A., Meyer, H., Kartoziia, A., Maggioni, F., and Strauss, J.: Fluvial and
959 permafrost history of the lower Lena River, north-eastern Siberia, over late Quaternary time, *Sedimentology*, 70, 235–258,
960 <https://doi.org/10.1111/sed.13037>, 2023.
- 961 Schwark, L., Zink, K., and Lechterbeck, J.: Reconstruction of postglacial to early Holocene vegetation history in terrestrial
962 Central Europe via cuticular lipid biomarkers and pollen records from lake sediments, *Geology*, 30, 463–466,
963 [https://doi.org/10.1130/0091-7613\(2002\)030%253C0463:ROPTEH%253E2.0.CO;2](https://doi.org/10.1130/0091-7613(2002)030%253C0463:ROPTEH%253E2.0.CO;2), 2002.
- 964 Shur, Y., Hinkel, K. M., and Nelson, F. E.: The transient layer: implications for geocryology and climate-change science,
965 *Permafrost and Periglacial Processes*, 16, 5–17, <https://doi.org/10.1002/ppp.518>, 2005.
- 966 Smith, S. L., O'Neill, H. B., Isaksen, K., Noetzli, J., and Romanovsky, V. E.: The changing thermal state of permafrost, *Nat*
967 *Rev Earth Environ*, 3, 10–23, <https://doi.org/10.1038/s43017-021-00240-1>, 2022.
- 968 Strauss, J., Schirrmeister, L., Mangelsdorf, K., Eichhorn, L., Wetterich, S., and Herzsich, U.: Organic-matter quality of deep
969 permafrost carbon – a study from Arctic Siberia, *Biogeosciences*, 12, 2227–2245, <https://doi.org/10.5194/bg-12-2227-2015>,
970 2015.
- 971 Strauss, J., Biasi, C., Sanders, T., Abbott, B. W., von Deimling, T. S., Voigt, C., Winkel, M., Marushchak, M. E., Kou, D.,
972 Fuchs, M., Horn, M. A., Jongejans, L. L., Liebner, S., Nitzbon, J., Schirrmeister, L., Walter Anthony, K., Yang, Y., Zubrzycki,
973 S., Laboor, S., Treat, C., and Grosse, G.: A globally relevant stock of soil nitrogen in the Yedoma permafrost domain, *Nat*
974 *Commun*, 13, 6074, <https://doi.org/10.1038/s41467-022-33794-9>, 2022.
- 975 Strauss, J., Fuchs, M., Hugelius, G., Miesner, F., Nitze, I., Opfergelt, S., Schuur, E., Treat, C., Turetsky, M., Yang, Y., and
976 Grosse, G.: Organic matter storage and vulnerability in the permafrost domain, in: *Encyclopedia of Quaternary Science*,
977 Elsevier, 399–410, <https://doi.org/10.1016/B978-0-323-99931-1.00164-1>, 2025.

- 978 Struck, J., Roettig, C. B., Faust, D., and Zech, R.: Leaf waxes from aeolianite–paleosol sequences on Fuerteventura and their
979 potential for paleoenvironmental and climate reconstructions in the arid subtropics, *E&G Quaternary Science Journal*, 66, 109–
980 114, <https://doi.org/10.5194/egqsj-66-109-2018>, 2018.
- 981 Stuiver, M. and Reimer, P. J.: Extended 14C Data Base and Revised CALIB 3.0 14C Age Calibration Program, *Radiocarbon*,
982 35, 215–230, <https://doi.org/10.1017/S0033822200013904>, 1993.
- 983 Thomas, C. L., Jansen, B., van Loon, E. E., and Wiesenberg, G. L. B.: Transformation of n-alkanes from plant to soil: a review,
984 *SOIL*, 7, 785–809, <https://doi.org/10.5194/soil-7-785-2021>, 2021.
- 985 Tipple, B. J. and Pagani, M.: A 35 Myr North American leaf-wax compound-specific carbon and hydrogen isotope record:
986 Implications for C4 grasslands and hydrologic cycle dynamics, *Earth and Planetary Science Letters*, 299, 250–262,
987 <https://doi.org/10.1016/j.epsl.2010.09.006>, 2010.
- 988 Ulyantsev, A. S., Romankevich, E. A., Bratskaya, S. Yu., Prokuda, N. A., Sukhoverkhov, S. V., Semiletov, I. P., and Sergienko,
989 V. I.: Characteristic of quaternary sedimentation on a shelf of the Laptev Sea according to the molecular composition of n-
990 alkanes, *Dokl. Earth Sc.*, 473, 449–453, <https://doi.org/10.1134/S1028334X17040158>, 2017.
- 991 Vonk, J. E., Fritz, M., Speetjens, N. J., Babin, M., Bartsch, A., Basso, L. S., Bröder, L., Göckede, M., Gustafsson, Ö., Hugelius,
992 G., Irrgang, A. M., Juhls, B., Kuhn, M. A., Lantuit, H., Manizza, M., Martens, J., O'Regan, M., Suslova, A., Tank, S. E.,
993 Terhaar, J., and Zolkos, S.: The land–ocean Arctic carbon cycle, *Nat Rev Earth Environ*, 6, 86–105,
994 <https://doi.org/10.1038/s43017-024-00627-w>, 2025.
- 995 Walter Anthony, K. M., Zimov, S. A., Grosse, G., Jones, M. C., Anthony, P. M., Iii, F. S. C., Finlay, J. C., Mack, M. C.,
996 Davydov, S., Frenzel, P., and Frolking, S.: A shift of thermokarst lakes from carbon sources to sinks during the Holocene
997 epoch, *Nature*, 511, 452–456, <https://doi.org/10.1038/nature13560>, 2014.
- 998 Webb, E. E., Liljedahl, A. K., Cordeiro, J. A., Loranty, M. M., Witharana, C., and Lichstein, J. W.: Permafrost thaw drives
999 surface water decline across lake-rich regions of the Arctic, *Nat. Clim. Chang.*, 12, 841–846, <https://doi.org/10.1038/s41558-022-01455-w>, 2022.
- 1000
- 1001 Webb, H., Fuchs, M., Abbott, B. W., Douglas, T. A., Elder, C. D., Ernakovich, J. G., Euskirchen, E. S., Göckede, M., Grosse,
1002 G., Hugelius, G., Jones, M. C., Koven, C., Kropp, H., Lathrop, E., Li, W., Loranty, M. M., Natali, S. M., Olefeldt, D., Schädel,
1003 C., Schuur, E. A. G., Sonntag, O., Strauss, J., Virkkala, A.-M., and Turetsky, M. R.: A Review of Abrupt Permafrost Thaw:
1004 Definitions, Usage, and a Proposed Conceptual Framework, *Curr Clim Change Rep*, 11, 7, <https://doi.org/10.1007/s40641-025-00204-3>, 2025.
- 1005
- 1006 Weber, J. and Schwark, L.: Epicuticular wax lipid composition of endemic European *Betula* species in a simulated
1007 ontogenetic/diagenetic continuum and its application to chemotaxonomy and paleobotany, *Science of The Total Environment*,
1008 730, 138324, <https://doi.org/10.1016/j.scitotenv.2020.138324>, 2020.
- 1009 Wolter, J., Lantuit, H., Herzschuh, U., Stettner, S., and Fritz, M.: Tundra vegetation stability versus lake-basin variability on
1010 the Yukon Coastal Plain (NW Canada) during the past three centuries, *The Holocene*, 27, 1846–1858,
1011 <https://doi.org/10.1177/0959683617708441>, 2017.
- 1012 Wolter, J., Jones, B. M., Fuchs, M., Breen, A., Bussmann, I., Koch, B., Lenz, J., Myers-Smith, I. H., Sachs, T., Strauss, J.,
1013 Nitze, I., and Grosse, G.: Post-drainage vegetation, microtopography and organic matter in Arctic drained lake basins, *Environ.*
1014 *Res. Lett.*, 19, 045001, <https://doi.org/10.1088/1748-9326/ad2eeb>, 2024.

- 1015 Wu, J., Mollenhauer, G., Stein, R., Köhler, P., Hefter, J., Fahl, K., Grotheer, H., Wei, B., and Nam, S.-I.: Deglacial release of
1016 petrogenic and permafrost carbon from the Canadian Arctic impacting the carbon cycle, *Nat Commun*, 13, 7172,
1017 <https://doi.org/10.1038/s41467-022-34725-4>, 2022.
- 1018 Yang, S., Anthony, S. E., Jenrich, M., in 't Zandt, M. H., Strauss, J., Overduin, P. P., Grosse, G., Angelopoulos, M., Biskaborn,
1019 B. K., Grigoriev, M. N., Wagner, D., Knoblauch, C., Jaeschke, A., Rethemeyer, J., Kallmeyer, J., and Liebner, S.: Microbial
1020 methane cycling in sediments of Arctic thermokarst lagoons, *Global Change Biology*, 29, 2714–2731,
1021 <https://doi.org/10.1111/gcb.16649>, 2023.
- 1022 Zech, M., Andreev, A., Zech, R., Müller, S., Hambach, U., Frechen, M., and Zech, W.: Quaternary vegetation changes derived
1023 from a loess-like permafrost palaeosol sequence in northeast Siberia using alkane biomarker and pollen analyses, *Boreas*, 39,
1024 540–550, <https://doi.org/10.1111/j.1502-3885.2009.00132.x>, 2010.
- 1025 Zech, M., Lerch, M., Bliedtner, M., Bromm, T., Seemann, F., Szidat, S., Salazar, G., Zech, R., Glaser, B., Haas, J. N., Schäfer,
1026 D., and Geitner, C.: Revisiting the subalpine Mesolithic site Ullafelsen in the Fotsch Valley, Stubai Alps, Austria – new insights
1027 into pedogenesis and landscape evolution from leaf-wax-derived n-alkanes, black carbon and radiocarbon dating, *E&G*
1028 *Quaternary Sci. J.*, 70, 171–186, <https://doi.org/10.5194/egqsj-70-171-2021>, 2021.
- 1029 Zimmermann, M., Erikson, L. H., Gibbs, A. E., Prescott, M. M., Escarzaga, S. M., Tweedie, C. E., Kasper, J. L., and Duvoy,
1030 P. X.: Nearshore bathymetric changes along the Alaska Beaufort Sea coast and possible physical drivers, *Continental Shelf*
1031 *Research*, 242, 104745, <https://doi.org/10.1016/j.csr.2022.104745>, 2022.

1032

1033